APPLICATION OF COMPUTATIONAL FLUID DYNAMICS IN THE STUDY OF AGRICULTURAL DIRECT SOLAR DRYERS

By

KOBUSINGE SARAH

BU/GS21/MIM/4

A RESEARCH DISSERTATION SUBMITTED TO THE DIRECTORATE OF GRADUATE STUDIES, RESEARCH AND INNOVATIONS IN PARTIAL FULFILLMENT OF THE REQUIREMENTS FOR THE AWARD OF THE DEGREE OF MASTER OF SCIENCE IN INDUSTRIAL MATHEMATICS OF BUSITEMA UNIVERSITY

OCTOBER , 2024

DECLARATION

I Kobusinge Sarah, hereby declare that to the best of my knowledge, this dissertation entitled 'APPLICATION OF COMPUTATIONAL FLUID DYNAMICS IN THE STUDY OF AGRICULTURAL DIRECT SOLAR DRYERS' is truly my original work and has never been submitted to any other university for the award of a degree or any other qualifications.

Name: KOBUSINGE SARAH

Registration Number: BU/GS21/MIM/4

Signature: KSB.

Date 29th/10/2024

APPROVAL

This Dissertation entitled, "Application of Computational Fluid Dynamics in the study of Agricultural Direct Solar Dryers" is submitted as a Partial Fulfillment for the Award of the degree of Master of Science in Industrial Mathematics of Busitema University, with the approval of the following academic supervisors.

1. Prof. Semwogerere Twaibu

Department of Computer Engineering and Informatics

Busitema University (U)

Signature.....

Date.....30/10/2024

2. Dr. Muhumza Asaph Keikara

Department of Mathematics, Faculty of Science and Education

Busitema University (U)

Signature.....

Date.....29/10/2024

APPROVAL

This Dissertation entitled, "Application of Computational Fluid Dynamics in the study of Agricultural Direct Solar Dryers" is submitted as a Partial Fulfillment for the Award of the degree of Master of Science in Industrial Mathematics of Busitema University, with the approval of the following academic supervisors.

1. Prof. Semwogerere Twaibu

Department of Computer Engineering and Informatics

Busitema University (U)

Signature.....

Date.....30/10/2024

2. Dr. Muhumza Asaph Keikara

Department of Mathematics, Faculty of Science and Education

Busitema University (U)

Signature.....

Date.....29/10/2024

DEDICATION

I would like to dedicate this work to the Almighty God for his grace, favour, and wisdom that he has granted me, to my Father Mzee Kimera Anthony, my late mother Nassanga Florence, and all my brothers and sisters who have always strived to show me the true value of Education, my dear husband Dr. Mukuzi Muheereza, children and entire family, for all your support and inspiration.

ACKNOWLEDGMENT

First and foremost, I am immensely grateful to the almighty God for bestowing me the gifts of life, good health, wisdom, provision, and protection throughout my academic journey.For it is only by His grace that I have been able to come this far.

I wish to express my gratitude to Busitema University, specifically the Faculty of Science and Education, Nagongera Campus, for allowing me to undertake this course.

My sincere and deepest gratitude goes to my supervisors, Prof. Semwogerere Twaibu and Dr. Muhumuza Asaph Keikara . Their advice, continuous stream of ideas, insightful criticisms, and encouragement helped me write this dissertation. They have been inspirational in allowing me to investigate while keeping me focused and, at the same time, free. Their interest helped my enthusiasm towards completing this research. Special thanks to the Department of Mathematics Busitema University staff for the significant impact on education.

To the Head of the Department of Mathematics, Dr. Abubakar Mwasa, thank you for always attending our seminar series physically and encouraging us to continue moving forward since it is a sole journey. Dr. Rebecca Muhumuza Nalule , Dr. Fulgensia Mbabazi, Mr. Stephen Kadedesya and Dr. Joseph Ddumba Lwanyaga, thank you for your valuable support. I am deeply grateful to Dr. Anselm Oyem and Dr. Annet Kyomuhangi for their technical advice and continuous support during our research presentation. Your guidance
was instrumental in shaping this work, and I genuinely appreciate your contributions.

I want to express my heartfelt gratitude to my MIM classmates at Busitema University, Diana Nekesa, William Lyinda, Samuel Iziziga, Samuel Kirabe, and Emmanuel Wafula. Your camaraderie and support have been a source of strength throughout our academic journey. I am truly grateful for your friendship and the memories we have shared. I wish you all the best in your future endeavors, and may the blessings of God accompany you in all your career pursuits.

Finally, my gratitude goes to Dr. Mukuzi Muheereza, my husband; Kusiima Harriet, my sister; and my friends, Tulirinya John and Rogers Waibi, Orishaba Patience, Revious Mbogo, and Vivian Kansiime for for spiritual, moral, and financial support.

TABLE OF CONTENTS

LIST OF FIGURES

ACRONYMS AND ABBREVIATIONS

CFD	:	Computational Fluid Dynamics
ANSYS	:	Analysis System
ISD	:	Indirect Solar Dryer
ETSC	:	Evacuated Tube Solar Collector .
PCM	:	Phase Change Materials
ANFIS	:	Adaptive-Network-Based Fuzzy Inference System
ANN	:	Artificial Neural Networks
FEM	:	Finite Element Method
FVM	:	Finite Volume Method
MATLAB	:	MATrix LABoratory
NS	:	Navier Stokes
NRI	:	Natural Research Institute
PDEs	:	Partial Differential Equations.
SDGs	:	Social Development Goals

NOMENCLATURE

T	Temperature	K
ρ	Density of the fluid	$kg\,m^{-3}$
$\vec{u}$	Fluid Velocity	$m\,s^{-1}$
p	Pressure	Pa
$\vec{F}$	Body Force	N
$\vec{g}$	acceleration due to gravity	$m\,s^{-2}$
k	Thermal Conductivity	$W\,m^{-1}K^{-1}$
C_p	Specific Heat Capacity at constant pressure	$J\,kg^{-1}\cdot K$
τ	Shear Stress	$Pa\,s^{-2}$
μ	Dynamic Viscosity	$Pa\cdot s$
α	Thermal diffusivity	m^2/s

ABSTRACT

ThisstudyexploredtheapplicationofComputationalFluidDynamics(CFD)ininvestigating the efficiency and airflow patterns of three different agricultural solar dryers. The dryers analyzed include trapezium, rectangular prism, and triangular prism top shaped designs. The primary objective was to optimize airflow uniformity and temperature distribution, which are critical factors for improving drying efficiency and product quality. CFD simulations were conducted using COMSOL Multiphysics version 6.2, with models based on the Navier-Stokes equations for fluid flow and the energy equation for heat transfer. The results identified the third design, that is, Triangular Prism geometry top shaped, as the most effective dryer design in terms of drying uniformity and efficiency, thus providing valuable insights for improving post-harvest handling and reducing food losses. The study concluded that the trapezium design offers the best performance in terms of uniform drying and energy efficiency. The practical implication of these findings is the potential reduction of post-harvest losses by improving drying technologies in agriculture. The triangular-shaped dryer provides a cleaner, more efficient drying process, promoting food preservation and supporting the sustainability of small-scale farmers in developing regions. This contributes to food security and climate change mitigation by reducing dependence on traditional, fossil-fuel-powered drying methods.

Chapter 1

Introduction

1.1 Background

Most sustainable economic developed countries depends on agriculture where it often accounts for a significant portion of the GDP and employment (Pawlak & Kołodziejczak, 2020). Post-harvest losses is one of the major problem faced by most agricultural sectors in the world. Approximately one-third of the food produced globally for human consumption is lost or wasted (FAO, 2017). The Food and Agriculture Organization (FAO) estimates that about one-third of the food produced worldwide for human consumption is lost or wasted. A significant amount of this waste happens during post-harvest handling, storage, and processing (Tadesse, 2020).

Human beings face a challenge in maintaining equilibrium between agricultural production and consumption (Marten, 2010). Enhancing agricultural production to accommodate population growth can address this disparity in food availability. Poor transportation, lack of suitable technology, poor yield storage, improper fertilization, and high post-harvest losses, among other factors, causing significant food loss in developing countries, ranging from 10 to 40% (Crist, Mora, & Engelman, 2017).

The drying of agricultural produce reduces the moisture content of products, thereby extending their shelf life and maintaining quality. Agricultural produce preservation encompasses methods that enhance food's resistance to microbial growth and decelerate fat oxidation, slowing decomposition and the onset of rancidity (Amit, Uddin, Rahman, Islam, & Khan, 2017). Rancidity leads to undesirable changes in flavor, smell,

and sometimes the appearance of fats and oil-containing foods, making them unsuitable for consumption.

Traditional drying methods, such as open sun drying, are widely practiced due to their low cost and simplicity (Tiwari, 2016). However, these methods are inefficient, time-consuming, and often result in significant losses due to contamination, weather fluctuations, and uneven drying.

1.1.1 Traditional Drying Method

Open sun drying is one of the conventional approach of food preservation where products like apples,pineapples, fish, and cereals are exposed to the sun and natural air (Sahdev, 2014). This process relies on solar radiation to evaporate moisture from the food. The items are typically spread out on a flat surface, such as mats, trays, or concrete floors, to maximize exposure to sunlight and airflow. The drying time can vary from a few hours to several days, depending on factors like the type of food, the thickness of the pieces, and the intensity of the sunlight (Babu, Kumaresan, Raj, & Velraj, 2018). This method is economical, requiring minimal equipment and energy, making it suitable for small-scale farmers and communities in areas with plentiful sunlight. An example of open sun drying is shown in Figure 1.1.

However, open sun drying has several drawbacks. It is highly dependent on weather conditions, making it unreliable in regions with unpredictable or rainy weather (OrtizRodríguez, Condorí, Durán, & García-Valladares, 2022). The process also exposes food to contamination from dust, insects, and animals, posing significant hygiene concerns (Runganga, 2019). Additionally, uneven drying can occur due to variations in sunlight and airflow, potentially leading to spoilage or reduced quality of the dried products. Despite these challenges, open sun drying remains widely used in many parts of the world due to its simplicity and low cost (Mohana et al., 2020).

In open sun drying, short-wavelength solar energy strikes the uneven surface of the crop. A portion of this energy is reflected, while the rest is absorbed by the crop surface, depending on its color. The absorbed energy is transformed into thermal energy, causing the crop's temperature to rise. This leads to the emission of long-wavelength radiation from the crop

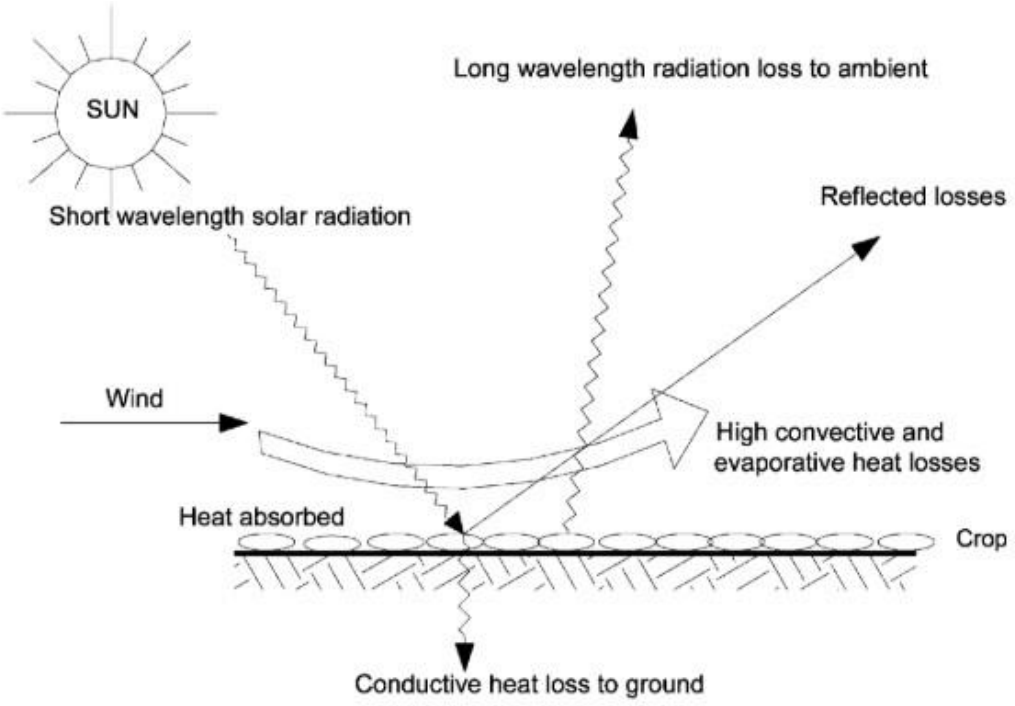

Figure 1.1: This figure demonstrates the Open Sun Drying process (Visavale, 2012).

surface into the surrounding moist air. Along with this radiation loss, convective heat loss occurs as wind blows over the moist crop surface. Moisture evaporates in the form of evaporative losses, resulting in the drying of the crop (Sharma, Chen, & Lan, 2009).

A portion of the absorbed thermal energy is conducted into the product's interior, leading to an increase in temperature and the generation of water vapor inside the crop. This vapor then diffuses toward the surface and ultimately releases thermal energy through evaporation. In the initial stages, moisture removal is rapid because the excess surface moisture creates a wet surface exposed to the drying air. As the process continues, the drying rate is determined by how quickly moisture within the product

moves to the surface through diffusion, which varies depending on the type of product (El-Mesery, El-Seesy, Hu, & Li, 2022).

1.1.2 Solar Drying Technologies

Solar drying technologies represent a significant advancement over traditional drying methods by providing a controlled and efficient means of drying agricultural produce. These technologies capitalize on solar energy, a renewable resource, to produce the necessary heat for the drying process. By utilizing solar energy, these technologies reduce the reliance on fossil fuels, which are not only finite but also contribute to greenhouse gas emissions (Holechek, Geli, Sawalhah, & Valdez, 2022). As a result, embracing solar drying technologies can be instrumental in reducing climate change impacts and supporting sustainable agricultural practices.

Solar dryers come in various types, each utilizing solar energy in distinct ways. Indirect solar dryers use solar collectors to heat air, which is then circulated through a drying chamber. Hybrid solar dryers combine solar energy with additional heat sources, ensuring steady drying even in cloudy conditions. Direct solar dryers, on the other hand, expose products directly to solar radiation. These direct dryers are highly efficient because they use sunlight to heat the air around the agricultural product, enhancing both drying effectiveness and product quality (Mohana et al., 2020).

Direct solar dryers offer numerous advantages over traditional sun drying methods. One of the primary benefits is the provision of a cleaner and more hygienic drying environment. Traditional sun drying often exposes produce to dust, insects, and other contaminants, whereas direct solar dryers protect the produce within a controlled environment. Additionally, direct solar dryers significantly reduce drying time compared to traditional methods, which can be particularly advantageous in regions with high

humidity or frequent rainfall where drying times are otherwise prolonged (Mohana et al., 2020).

By enhancing the efficiency of the drying process, direct solar dryers help mitigate postharvest losses. In many developing regions, a significant portion of agricultural produce is lost due to inadequate drying, which leads to spoilage. Solar dryers ensure that more produce can be preserved in good condition, thus increasing the quantity of marketable goods. This not only benefits farmers by increasing their income but also contributes to food security by reducing waste and ensuring a more stable supply of dried produce (Ssemwanga, Makule, & Kayondo, 2020).

Furthermore, the use of solar dryers supports environmental sustainability. By reducing the need for fossil fuel-based drying methods, solar dryers decrease the carbon footprint associated with food processing. This is particularly relevant in the context of global efforts to combat climate change (Ssemwanga et al., 2020). Additionally, solar dryers can be constructed from locally available materials, making them accessible and affordable for small-scale farmers. The promotion of solar drying technologies can therefore have far-reaching impacts, from improving agricultural efficiency and economic stability to fostering environmental stewardship (see Figure 1.2).

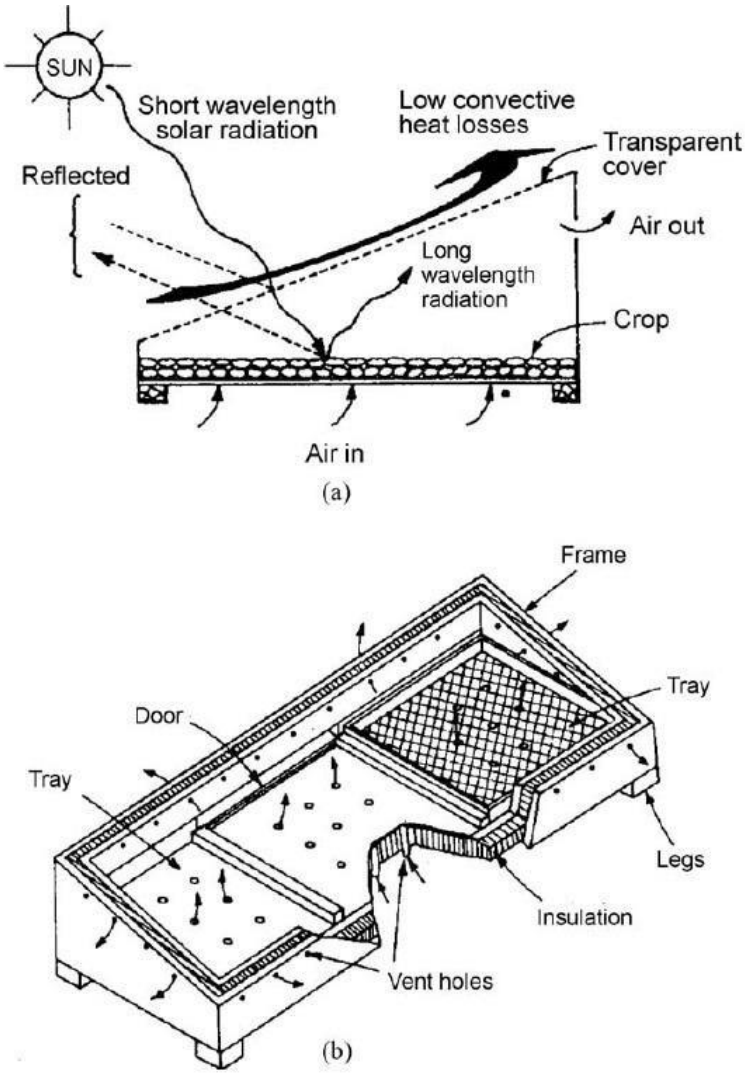

Figure 1.2: This figure shows direct solar drying of agricultural food products (Sadeghi et al., 2012).

1.1.3 Computational Fluid Dynamics (CFD): A Tool for Optimization

Computational Fluid Dynamics (CFD) has emerged as a powerful tool for optimizing various engineering applications, including the design of direct solar dryers (Malekjani & Jafari, 2018). CFD allows researchers to create detailed simulations of these processes, providing insights that are not easily obtainable through experimental methods alone. By leveraging CFD, engineers and scientists can enhance the performance of solar dryers, ensuring uniform drying, reducing energy consumption, and improving overall productquality.

At its essence, CFD focuses on solving the fundamental fluid mechanics equations, specifically the Navier-Stokes equations, which govern the motion of fluid substances (Schobeiri, 2010). This involves discretizing the equations over a computational grid or mesh that represents the physical domain of the problem. By iterating through these calculations, CFD software can predict how fluids will behave under various conditions, including the airflow patterns, temperature distribution, and heat transfer rates in a solar dryer.

Applying CFD to solar dryer design involves several critical steps. First, a geometric model of the dryer is created, encompassing all relevant components such as the drying chamber, air inlets, and outlets. Next, boundary conditions and initial conditions are defined to mimic the actual operating environment, such as ambient temperature, solar radiation, and airflow rates (Defraeye, 2014). CFD simulations are then run to analyze how air and heat move through the dryer. These simulations can reveal areas where airflow might be stagnating, causing uneven drying, or where temperature gradients might be too steep, potentially damaging the product being dried. By identifying these issues, researchers can modify the design to improve performance.

One of the key benefits of using CFD in the design of solar dryers is the ability to conduct parametric studies efficiently. Engineers and scientists can vary design parameters, such as the size and shape of the dryer, the positioning of air inlets and outlets, and the material properties of the dryer walls, to observe how these changes affect performance. This capability enables the optimization of dryer design without the need for extensive physical prototyping, saving time and resources. Additionally, CFD allows for the exploration of innovative design concepts that might be impractical or too costly to test experimentally in the initial stages.

Furthermore, CFD provides valuable visualization tools that help researchers understand the intricate details of fluid flow and heat transfer within solar dryers. These visualizations can include contour plots of temperature and velocity fields,

streamlines showing airflow patterns, and animations that depict the dynamic changes in these fields over time. Such visual representations make it easier to communicate findings and design recommendations to stakeholders, including engineers, manufacturers, and end-users. Solar dryers harness solar energy to dehydrate agricultural products, preserving them for longer periods. The efficiency of these dryers hinges on the effective management of fluid flow and heat transfer processes (Ndukwu et al., 2022).

In summary, CFD is a vital resource for optimizing the design of direct solar dryers, leading to more economical,efficient, and sustainable drying solutions.

1.2 Statement of the Problem

Agricultural productivity is often hindered by post-harvest losses, which can be significantly reduced through effective drying processes. Traditional sun drying methods, although common, are typically inefficient, prone to contamination, and heavily dependent on weather conditions. This inefficiency can lead to substantial quality degradation and economic losses for farmers. In light of these challenges, there is a growing need for more reliable and efficient drying technologies and systems. To optimize these systems, it is crucial to understand the airflow patterns and temperature distributions within the dryers, as these factors directly influence drying efficiency and product quality.

The application of Computational Fluid Dynamics (CFD) serves as an effective tool for analyzing and enhancing the performance of agricultural solar dryers. By modeling airflow and temperature distribution, CFD delivers valuable insights into the internal dynamics of various dryer designs.

1.3 Objectives of the Study

The study was guided by these main and specific objectives;

1.3.1 Main Objective

The main objective of this study is to apply Computational Fluid Dynamics in the design of agricultural direct solar dryers.

1.3.2 Specific Objectives

i. To analyze the airflow patterns within three different agricultural solar dryers.

ii. To investigate the temperature distribution inside three different agricultural solar dryers.

iii. To compare the three different agricultural solar dryers under study and advise on the best one.

1.4 Scope of Study

The scope of this study encompasses the comprehensive application of Computational Fluid Dynamics (CFD) to the design and analysis of agricultural direct solar dryers. The study focuses on three different types of solar dryers, chosen based on their prevalent use and potential for optimization in agricultural settings. The primary areas of investigation include the simulation of airflow patterns and temperature distributions within each dryer type.

In addition to the CFD simulations, the study undertakes a comparative analysis of the three solar dryer designs. This comparison is based on key performance indicators such as airflow uniformity, temperature distribution, and overall drying efficiency. The study also considers practical aspects such as ease of construction, cost-effectiveness, and suitability for different agricultural products. By integrating these factors, the research provides a holistic evaluation of each dryer type, offering recommendations for optimal design and implementation. The ultimate goal is to inform and guide the development

of more efficient and reliable solar drying technologies, thereby enhancing the preservation and quality of agricultural produce.

1.5 Significance

Despite the inherent advantages of solar drying technologies, their widespread adoption in agriculture has been hindered by several significant challenges. One of the primary obstacles is the lack of optimized designs tailored to different types of agricultural produce and varying climatic conditions. Many existing designs are either too generic or fail to achieve the necessary efficiency and uniformity in drying, leading to inconsistent product quality. High initial costs associated with setting up solar drying systems also pose a barrier, particularly for small-scale farmers in developing regions. Furthermore, limited technical knowledge and expertise in the design, operation, and maintenance of solar dryers prevent farmers from fully utilizing these technologies. This study addresses these issues by applying Computational Fluid Dynamics (CFD) to the design and optimization of agricultural direct solar dryers. By leveraging CFD's advanced simulation capabilities, this research aims to develop dryer designs that are not only highly efficient and effective but also cost-effective and straightforward to implement, thereby making them accessible to a broader range of users.

The motivation for this study is rooted in the urgent need to enhance the sustainability and resilience of the agricultural sector, which faces increasing pressures from climate change, population growth, and food security challenges. Improving the efficiency of post-harvest processing, particularly drying, can significantly reduce food losses that occur after harvest, thereby ensuring that more produce reaches the market in good condition.

The reduction in food losses not only improves food security but also increases the income of farmers by preserving the quality and marketability of their products.

Furthermore, by encouraging the usage of sustainable energy sources like solar, this study aligns with global efforts to combat climate change and foster sustainable development. Solar drying technologies offer a clean, renewable, and eco-friendly solution that can mitigate the environmental impact of traditional drying methods, which often rely on fossil fuels. Thus, the findings and outcomes of this research have the potential to drive significant advancements in agricultural practices, contributing to a more sustainable and resilient food production system.

Chapter 2

Literature Review

The development and optimization of agricultural direct solar dryers have been the focus of extensive research, driven by the need to improve post-harvest handling and reduce crop losses. Traditional sun drying, while cost-effective, presents numerous challenges including vulnerability to weather conditions, contamination risks, and inconsistent drying rates. In response, solar dryer technologies have been developed, offering a controlled environment that enhances drying efficiency and product quality (Goel et al., 2024). The literature on solar dryers encompasses a wide range of studies, from basic design principles and material selection to advanced computational modeling and performance evaluation.

In this field of study, Computational Fluid Dynamics (CFD) has become an essential tool for understanding and enhancing the efficiency of solar dryers. By enabling researchers to simulate and examine complex airflow and heat transfer processes, CFD offers detailed insights that are challenging to achieve through experimental approaches alone. Numerous studies have employed CFD to investigate various aspects of solar dryer design, including airflow patterns, temperature distribution, and moisture removal rates. These studies have demonstrated the potential of CFD to identify design improvements that enhance drying efficiency and uniformity (Tu, Yeoh, Liu, & Tao, 2023). This literature review aims to synthesize existing research on the use of CFD in solar dryer design, highlighting key findings, methodologies, and gaps in the current knowledge. By doing so, it provides a solid foundation for the present study, which seeks to apply CFD to evaluate and compare three different types of agricultural solar dryers.

Demissie et al. (2019) conducted a study on design, development and CFD modeling of indirect solar food dryer to predict air flow and temperature distribution within the drying chamber, and validated the temperature distribution experimentally. The findings showed that the CFD model effectively predicts airflow and temperature distribution. However, the study did not consider the possible effects of changing environmental conditions on the dryer's performance, which may limit the broader applicability of the results.

Chavan, Vitankar, Shinde, and Thorat (2021) explored the design and optimization of a solar grain dryer using Computational Fluid Dynamics (CFD). The study addressed the inefficiencies of traditional open sun drying, such as improper utilization of solar energy and extended drying times that compromise product quality. The authors proposed a compact solar grain dryer and optimized its design for higher energy efficiency by simulating different configurations. The findings indicated that specific design modifications, including the introduction of fins, significantly improve dryer performance. However, a research gap exists in the experimental validation of these CFD simulations and the exploration of real-world application scenarios for the proposed designs.

Singh, Salhan, and Kumar (2021) effectively utilized CFD to simulate the performance of an indirect solar dryer, providing valuable insights into its thermal and dynamic behavior. The study stands out for its detailed analysis of various mass flow rates and their impact on parameters such as velocity and temperature profiles within the dryer, which are crucial for optimizing the drying process. However, while the simulations are thorough, their findings could benefit from a more extensive comparison with other types of solar dryers to highlight the relative advantages and potential drawbacks of the indirect forced convection design.

Adeniyi, Mohammed, and Aladeniyi (2012) presented a CFD analysis of a solar dryer box designed for preserving farm produce in Nigeria. The authors highlighted the need for cost-effective and efficient preservation methods that do not rely on electricity, emphasizing the benefits of solar drying for vitamin preservation.

Noh, Mat, and Ruslan (2018) conducted a study on CFD simulation of temperature and air flow Distribution inside Industrial Scale Solar Dryer, presenting a well-structured analysis of how different product arrangements and operating conditions affect temperature and airflow within a solar dryer. The study utilized CFD simulation via ANSYS Fluent to model these factors, demonstrating the efficiency of a zig-zag pallet arrangement and the benefits of intermittent active ventilation.

Stoppe, Neto, and dos Santos (2020) presented a comprehensive study on the use of Computational Fluid Dynamics (CFD) to enhance the efficiency of solar dryers for agricultural products. Their research demonstrated a thorough analysis of airflow patterns and their impact on drying rates by comparing fully opened and partially opened air inlet configurations.

Obayopo and Oluwasanmi (2019) conducted a study on the analysis of a direct solar dryer designed for fish preservation. The study successfully integrated numerical modeling using Computational Fluid Dynamics (CFD) with experimental validation to optimize the dryer's performance. The findings indicated that the use of CFD to simulate different dimensions and fan speeds is commendable as it helps in identifying the optimal configuration for uniform air distribution and temperature.

Benhamza, Boubekri, Atia, Hadibi, and Arıcı (2021) carried out an investigation on the effectiveness of solar chimneys and forced convection in improving the drying uniformity and temperature of an indirect solar dryer (ISD). The methodology employed included, experimental procedures, CFD simulations, and image processing for

analyzing results. The findings indicated a clear advantage in using forced convection at specific mass flow rates to enhance temperature uniformity.

Chaudhari, Kulkarni, and Sewatkar (2021) concentrated on utilizing computational fluid dynamics (CFD) to examine temperature distribution and airflow in a solar dryer equipped with auxiliary heaters and blowers. The results showed that the average temperature region inside the dryer increases as solar radiation intensifies throughout the day. The findings highlight the importance of integrating auxiliary heating to maintain consistent drying conditions and identify specific regions within the dryer that can be monitored for feedback control to optimize drying efficiency.

Güler et al. (2020) investigated the enhancement of thermal efficiency in a double pass solar air collector by incorporating iron mesh absorbers. The study employed both experimental and computational fluid dynamics (CFD) methods to design, manufacture, and test two versions of the solar dryer: one with a conventional double-pass configuration and another with the mesh modification. The experimental setup involved drying pepino fruit samples of varying thicknesses, with a focus on measuring thermal efficiency and analyzing the quality of the dried product, including phenolic content, total flavonoids, and antioxidant activity. The results demonstrated that the mesh modification significantly improves the collector's performance, achieving higher efficiency and better quality metrics for the dried fruit. The drying data is modeled using eight different mathematical models, with the logarithmic model providing the best fit for all experiments. The study concludes that integrating iron meshes in the solar air collector enhances its efficiency and the quality of the dried product.

In the research paper "Modeling and Improving the Performance of Cabinet Solar Dryer Using Computational Fluid Dynamics" by Ghaffari and Mehdipour (2015), a new approach for numerically modeling an entire cabinet solar dryer was presented. This

involved dividing the dryer into three principal sections: the collector, drying chamber, and chimney. The collector is modeled using energy and fluid flow equations, the drying chamber with computational fluid dynamics (CFD) due to its geometric complexity, and the chimney with comprehensive consideration of effective parameters. The numerical results align with experimental data, confirming the model's accuracy. The study finds that adding baffles optimizes the dryer by increasing efficiency and accelerating the drying process.

Getahun et al. (2021) discussed the advancements, challenges, and opportunities in the use of solar dryers for preserving fruits and vegetables. This included a comprehensive review of mathematical and computational models, particularly computational fluid dynamics (CFD), used to optimize the design and performance of solar dryers. The findings highlight that while CFD has been extensively used to study airflow, heat, and mass transfer in solar drying systems, it often neglects the quality aspects of the dried products. The paper emphasized the need for CFD models that can predict product quality in addition to traditional performance metrics like drying time and efficiency. This integrated approach could significantly improve the effectiveness of solar drying systems, ensuring better preservation of nutritional and sensory qualities of dried fruits and vegetables.

Iranmanesh, Akhijahani, and Jahromi (2020) under their paper titled "CFD modeling and evaluation of the performance of a solar cabinet dryer equipped with an evacuated tube solar collector and thermal storage system" investigated the efficiency and effectiveness of a solar cabinet drying system enhanced with a heat pipe evacuated tube solar collector (ETSC) and thermal storage system utilizing phase change materials (PCM). The study included thermal analysis, drying efficiency assessments, and Computational Fluid Dynamics (CFD) modeling, validated by experimental data. Experiments were conducted using apple slices dried at varying air flow rates with and without PCM. The findings indicated that incorporating PCM increased input thermal energy by up to 5.12% at

certain air flow rates, though higher flow rates diminished this benefit. The overall drying efficiency was highest at 39.9% for the system with PCM and an air flow rate of 0.025 kg/s. CFD simulations corroborated experimental results, confirming the enhanced performance of the dryer with PCM without compromising the quality of the dried products.

Jain, Sharma, Kumar, Sharma, and Palamanit (2019) investigated the design and performance of a domestic solar dryer using computational fluid dynamics (CFD) simulation. The study aimed to validate the design, perform an energy analysis, and compute various thermal parameters for the solar dryer. The methodology involved using ANSYS Fluent
14.0 software for the CFD simulation to analyze temperature and air flow distribution within the dryer at no load conditions. The key findings included a maximum air temperature of 326 K inside the dryer, an embodied energy of 339.015 kWh for the materials used, an energy payback time of 7.57 years, and a carbon credit value of INR 2055. The convective heat transfer coefficient ranged from 2.4 to 2.8 W/m²°C, and the coefficient of determination was 0.98, indicating a high correlation between predicted and experimental values. The study concluded that the CFD simulation effectively validates the dryer design, providing a cost-effective and efficient method for optimizing solar dryer performance.

In the research, titled “Simulation of Hybrid Solar Dryer” conducted by Yunus and AlKayiem (2013) explored the efficiency of a solar dryer integrated with a biomass burner as a backup heating source. The study utilized Computational Fluid Dynamics (CFD) to simulate the thermal and airflow fields within the dryer, aiming to enhance its design and performance. The simulation employed GAMBIT software for model and grid generation, and FLUENT software to analyze velocity and temperature distribution. The research involved validating CFD simulation results against experimental measurements, revealing

a close agreement. Key findings included identification of high-temperature spots with low air velocity indicating design flaws, and a detailed visualization of airflow and thermal distribution that could not be captured through experimental methods. The study concluded that hybrid mode, combining solar and biomass heating, is most effective for drying applications, providing insights for design improvements based on areas of low temperature and air velocity within the dryer.

Sonthikun et al. (2016) conducted a study focusing on the design, construction, and validation of a solar-biomass hybrid dryer for drying natural rubber sheets. The innovative dryer combines a solar collector with a drying chamber, a heat exchanger, and a biomass furnace, aiming to reduce biomass consumption by integrating solar energy. The study employed computational fluid dynamics (CFD) to simulate temperature and airflow distribution within the dryer. The experimental setup was validated by drying 100 natural rubber sheets, showing a significant reduction in moisture content from 34.26% to 0.34% in 48 hours. The results indicated that the hybrid dryer not only reduce drying time and biomass consumption but also improves the color and texture of the rubber sheets compared to traditional methods. The CFD simulations closely matched the experimental data, confirming the effectiveness of the dryer design and the utility of air circulating fans for uniform temperature distribution. The research concluded that the solar-biomass hybriddryerisaneconomicalandefficientalternativeforsmallholdersintherubberindustry.

Prakash, Laguri, Pandey, Kumar, and Kumar (2016) provided a comprehensive overview of different modelling techniques used to analyze and improve the performance of solar drying systems. The methodologies discussed include Computational Fluid Dynamics (CFD), Adaptive-Network-Based Fuzzy Inference System (ANFIS), Artificial Neural Networks

(ANN), Fuzzy Logic, and mathematical and thermal modelling. Each technique has specific applications, such as predicting drying rates, temperature, and moisture content, optimizing drying efficiency, and simulating air flow and heat transfer within the drying chamber. The research findings highlighted the effectiveness of these techniques in enhancing the design, efficiency, and prediction accuracy of solar dryers. For instance, CFD is useful for simulating fluid flow and heat transfer, while ANFIS and ANN are effective in handling nonlinear data interactions and predicting system behavior. Fuzzy Logic is noted for its ability to model uncertain and imprecise data. The paper also discussed the advantages of using these modelling techniques, such as saving time and resources, improving product quality, and supporting the development of more efficient and cost-effective solar drying systems.

Sanghi, Ambrose, and Maier (2018) developed a Computational Fluid Dynamics (CFD) model to simulate the drying process of corn in a solar cabinet dryer under different weather conditions. The methodology involves creating a CFD model that uses a dual-band spectrum to account for the absorption of solar radiation by corn and the greenhouse effect caused by glazing materials. The model was validated with experimental data collected from drying trials conducted in Kumasi, Ghana, involving a cabinet dryer loaded with white corn. Temperature and relative humidity within the dryer and ambient conditions were monitored. The model predicted the temperature, humidity, and air velocity profiles in the dryer, and its accuracy was assessed by comparing these predictions with experimental results. The study found that the model over-predicted temperature and humidity values but accurately captured airflow stagnation in the dryer. Under overcast conditions, the model predicted a 32% reduction in moisture removal compared to fair-weather conditions, demonstrating the significant impact of weather on drying performance. The findings suggest that the model can be used to optimize dryer design and improve drying efficiency by addressing airflow issues and adapting to specific environmental conditions.

Chauhan, Kumar, and Tekasakul (2015) conducted a review focusing on the use of various software tools to enhance the design, analysis, and optimization of solar drying systems. The review emphasizes the importance of software in developing mathematical models to predict the performance of different types of solar dryers, including direct, indirect, mixedmode, and hybrid systems. It discusses the application of computational fluid dynamics (CFD) using tools like ANSYS and FLUENT for airflow and temperature distribution analysis, and the use of MATLAB and FORTRAN for developing mathematical models to predict parameters such as crop temperature, moisture content, and drying rate. The paper highlights the utility of statistical software like SPSS, Sigma Plot V, and Statistica for data analysis and model validation. Key findings suggest that software applications can significantly improve the efficiency and accuracy of solar drying systems, reduce experimental time, and optimize design parameters. The review serves as a comprehensive resource for researchers and scientists in the field, providing insights into the simulation methodologies and performance evaluation techniques used in solar drying applications.

Vivekanandan, Periasamy, Babu, Selvakumar, and Arivazhagan (2021) explored the effectiveness of different solar greenhouse dryer shapes in achieving optimal temperature conditions. The research aimed to identify the best shape among six different designs: Parabola, Quonset, Modified Quonset, Pyramid, Igloo, and Tropical, each maintaining a consistent volume of 30 cubic feet. The methodology involved both experimental setups and computational fluid dynamics (CFD) simulations to measure and compare the internal temperatures of each shape under no load conditions. The results indicated that the Quonset shape was the most efficient, generating the highest internal temperatures, followed by the Tropical and Pyramid shapes. Specifically, the Quonset shape achieved temperatures up to

72°C in summer and 66°C in winter, outperforming the other designs by 7% in summer and 5% in winter. The study concluded that the Quonset shape is the ideal design for

solar greenhouse dryers, as it significantly enhances the drying efficiency by maintaining higher internal temperatures compared to the ambient atmosphere and other shapes.

Behera, Mohanty, and Mohanty (2023) focused on the development and analysis of a hybrid solar dryer designed for drying food products, specifically tomato slices. The methodology combined both experimental work and Computational Fluid Dynamics (CFD) simulations. The experimental setup included a flat plate solar collector and a drying chamber, with provisions for exhaust hot air recirculation to enhance efficiency. Experiments were conducted to measure temperatures at various points in the system, both during daytime using solar energy and at night using an auxiliary electric coil. CFD simulations were used to model and validate the thermal performance and airflow within the dryer. The findings indicate that the maximum efficiency of the solar collector reached 74.1% with exhaust hot air recirculation, and 66.96% without it. The drying efficiency was calculated at 32.89%, with the collector efficiency factor being 0.987. The study shows good agreement between experimental and simulated results, validating the effectiveness of the hybrid solar dryer, which is also lightweight, portable, and suitable for use in food processing industries.

Mukanema and Simate (2023) investigated the temperature and airflow dynamics within a natural convection solar tunnel dryer with a bare flat-plate chimney using Computational Fluid Dynamics (CFD) simulations. The objective was to identify areas of improvement for enhanced dryer performance. The dryer model was created using SOLIDWORKS 2016, and simulations were conducted to assess temperature distribution and airflow. The study revealed that the chimney loses heat, causing a reduction in airflow and drying efficiency. It also identified air recirculation in the collector and pressure losses as air moves from the drying chamber to the chimney. Experimental validation showed a good agreement with simulation results, with a mean relative

deviation of 5.1%. The study suggests insulating and glazing the chimney and using a curved joint between the chimney and drying chamber to improve performance. The CFD approach demonstrated its effectiveness in predicting temperature and airflow distribution, paving the way for better design of solar dryers.

2.1 Research Gap

The literature review reveals several research gaps in the application of Computational Fluid Dynamics (CFD) for agricultural solar dryer design, particularly in the context of achieving the general objective of our study. While numerous studies have demonstrated the efficacy of CFD in predicting airflow patterns and temperature distribution, there remains a significant gap in the comprehensive comparison of different types of solar dryers under varying environmental conditions. Most existing research focuses on specific dryer designs or individual performance parameters without addressing the holistic performance of different dryer types in diverse real-world scenarios (Pandey, Kumar, & Sharma, 2024). Additionally, there is a need for integrating product quality metrics into CFD models to ensure that the drying process not only optimizes efficiency but also preserves the nutritional and sensory qualities of the agricultural products (Adnouni et al., 2023). Hence, this study addresses these gaps through a detailed analysis and comparison of airflow patterns, temperature distribution in multiple solar dryer designs providing a more robust foundation for recommending the most effective dryer for agricultural use.

Chapter 3

Materials and Methods

3.1 Introduction

This chapter outlines the materials and methodologies employed in the study to achieve the objectives of analyzing airflow patterns and temperature distributions within three different designs of agricultural direct solar dryers using Computational Fluid Dynamics (CFD). The chapter details the design and selection of the solar dryers, the development and validation of the CFD models, and the parameters and conditions used in the simulations.

Additionally, the procedures for the comparative analysis of the dryers are described.

3.2 Solar Dryer Designs

Three distinct designs of agricultural solar dryers were selected for this study. These designs are shown in Figures 3.1, 3.2 and 3.3. Each dryer design was chosen based on its unique design characteristics and prevalent usage in agricultural drying applications.

3.3 CFD Model Development

3.3.1 Geometry and Mesh Generation

The geometries of the three solar dryers were created using Spaceclaim software (version 20), replicating real-world dimensions and configurations. The models were then imported into a CFD software package called COMSOL Multiphysics (version 6.2),

where the computational domain was discretized into a fine mesh to capture detailed airflow and temperature variations.

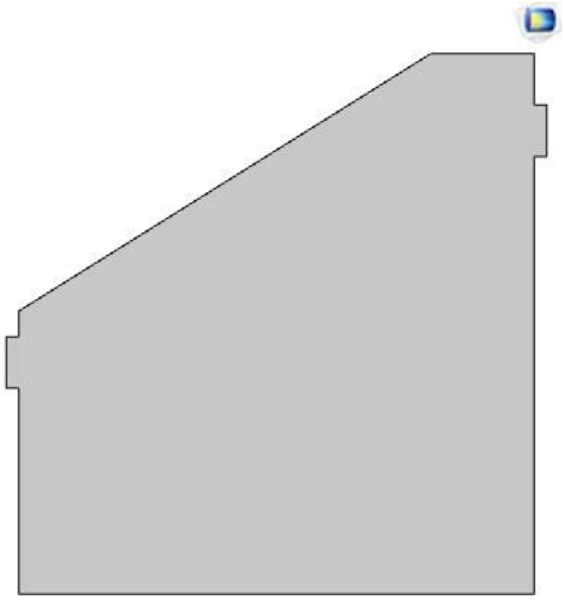

Figure 3.1: Trapezium geometric top shaped design (case 1) of the agricultural solar dryer.

Figure 3.2: Rectangular prism geometric top shaped design (case 2) of the agricultural solar dryer.

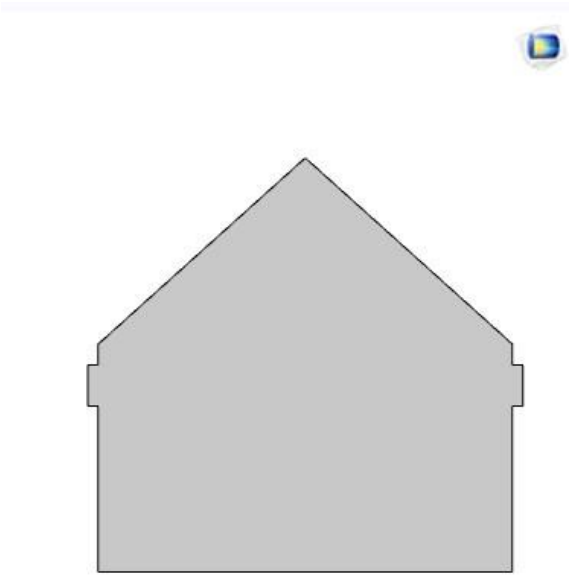

Figure 3.3: Triangular prism geometric top shaped design (case 3) of the agricultural solar dryer.

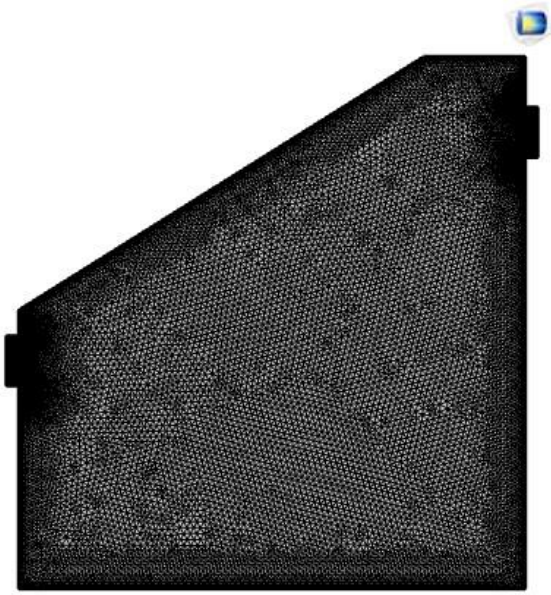

Figure 3.4: Mesh for the trapezium geometric top shaped design (case 1) of the agricultural solar dryer.

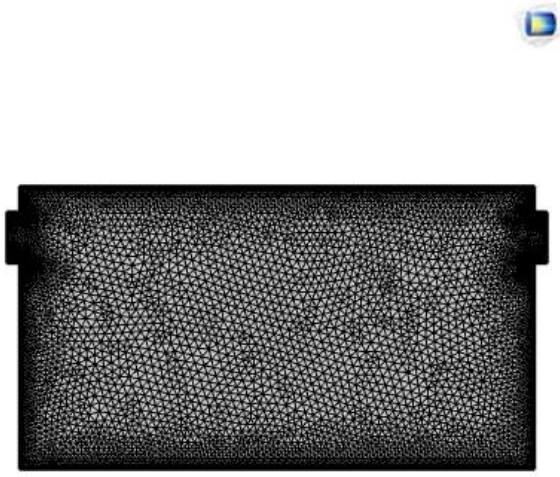

Figure 3.5: Mesh for the rectangular prism geometric top shaped design (case 2) of the agricultural solar dryer.

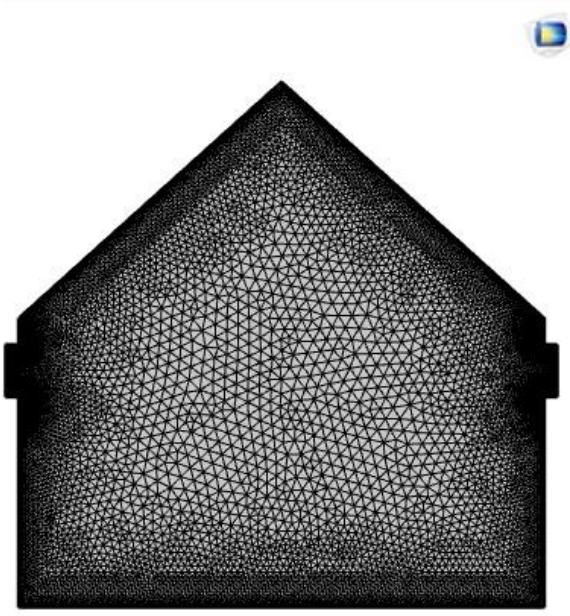

Figure 3.6: Mesh for the triangular prism geometric top shaped design (case 3) of the agricultural solar dryer.

3.3.2 Assumptions

The CFD simulations were based on the Navier-Stokes equations for fluid flow and the energy equation for heat transfer. The following assumptions were made to simplify the model:

i. Unsteady-state condition, where the variables change with time. ii. Incompressible airflow, where the density of air is constant. iii. Uniform material properties for the casing of the dryers. iv. Laminar flow of air inside the dryer. v Newtonian flow, where the viscosity of air is constant.

3.4 Mathematical Formulation

3.4.1 Governing Equations

For all types of flow, Computational Fluid Dynamics (CFD) solves the conservation equations for mass and momentum. When dealing with flows involving heat transfer or compressibility, an additional equation for energy conservation is also solved. These equations are;

Continuity equation:

$$\frac{\partial \rho}{\partial t} + \nabla \cdot (\rho \vec{v}) = 0 \tag{3.1}$$

where; ρ is air density (kg/m^3), t is time (s), and $\vec{v}$ is the air velocity vector.

Since the flow is assumed to be incompressible, it implies that $\frac{\partial \rho}{\partial t} = 0$. Therefore, equation (3.1) becomes;

$$\nabla \cdot \vec{v} = 0 \tag{3.2}$$

Momentum Conservation Equation

$$\frac{\partial (\rho \vec{v})}{\partial t} + \nabla \cdot (\rho \vec{v} \vec{v}) = -\nabla p + \nabla \cdot \tau + \rho \vec{g} + \vec{F} \tag{3.3}$$

where; p is dynamic pressure (Pa), $\vec{f}$ is the volume force vector, $\vec{g}$ acceleration due to gravity, and τ is shear stress tensor or deviatoric stress tensor which is defined as;

$$\tau = \mu(\nabla\vec{v} + (\nabla\vec{v})^T) - \frac{2}{3}\mu(\nabla\cdot\vec{v})I \tag{3.4}$$

where; μ is viscosity ($Pa.s/m^2$), I is unit tensor, $(\nabla\vec{v})$ is dyadic tensor, and $(\nabla\vec{v})^T$ is the transpose of dyadic tensor.

Considering incompressibilty of the flow, it implies that $(\nabla\vec{v})^T = \nabla\cdot\vec{v} = 0$, hence equation (3.4) simplifies to;

$$\tau = \mu\nabla\vec{v} \tag{3.5}$$

Assuming zero volume force vector, equation (3.3) becomes;

$$\frac{\partial(\rho\vec{v})}{\partial t} + \nabla\cdot(\rho\vec{v}\vec{v}) = -\nabla p + \nabla\cdot\tau + \rho\vec{g} \tag{3.6}$$

Substituting equation (3.5) into equation (3.6) yields;

$$\frac{\partial(\rho\vec{v})}{\partial t} + \nabla\cdot(\rho\vec{v}\vec{v}) = -\nabla p + \nabla\cdot(\mu\nabla\vec{v}) + \rho\vec{g} \tag{3.7}$$

Since the flow is assumed Newtonian, it means that the viscosity □ is constant, hence equation (3.7) becomes;

□(□□□®) 2® + □□®(3.8)
+ □ · (□□®□®) = −□□ + □□ □
□□

Energy Conservation Equation

□(□□□□□)
_____ + □ · (□□□□□□®) = □ · (□□□□) + □□ (3.9)
□□

where; □□ is specific heat capacity at constant pressure, □ is temperature, □ is thermal conductivity and □□ is the heat source term which is modeled to capture heat by radiation called the inward heat flux.

□□
□□□ ___ + □□□□ · (®□□□) = □ · (□□□□) + □□ (3.10)
□□

But,

□ · (®□□□) = □(□ · ®□) + □® · □□ (3.11)

Due to incompressibility of the flow (□ · ®□ = 0), hence equation (3.11) reduces to;

□ · (®□□□) = □® · □□ (3.12)

Equation (3.10) now becomes;

□□
□□□ ___ + □□□□□® · □□ = □ · (□□□□) + □□ (3.13)
□□

Assuming a constant value for the thermal conductivity, □, equation (3.13) becomes;

□□
□□□ ___ + □□□□□® · □□ = □□2□ + □□ (3.14)
□□

Which further simplifies to;

$$\frac{\partial T}{\partial t} + \nabla \cdot (\mathbf{v} T) = \alpha \nabla^2 T + \frac{q}{\rho c_p} \tag{3.15}$$

where; $\alpha = \frac{k}{\rho c_p}$, α is called the thermal diffusivity and $\frac{q}{\rho c_p} = \frac{Q}{\rho c_p}$

3.4.2 Boundary Conditions

Appropriate boundary conditions were set for each model as follows;

(i) Inlet Boundary Condition.

- Inlet air velocity is set at 0.5 m/s, $\mathbf{v}_{inlet} = 0.5 m/s$.
- Temperature at the inlet is defined as 293.15 K, $T_{inlet} = 293.15K$.

(ii) Outlet pressure (zero pressure gradient). A zero-pressure gradient is imposed at the outlet, meaning the outlet is set to have a constant pressure value without gradients.

$\frac{\partial p}{\partial n} = 0$

(iii) Wall Boundary Condition

- The wall temperatures are defined based on the absorption of solar radiation.

T_{wall} = function of solar radiation absorption

- A no-slip condition is applied, meaning the velocity of the airflow is set to zero at the walls. $\mathbf{v}_{wall} = 0$

(iv) Inward Heat Flux

- An inward heat flux of 1000 W/m^2 is applied at the transparent glass, simulating

solar radiation energy input into the system. $□_{glass}$ = 1000□/□^{2}

Chapter 4

Results and Discussion

4.1 Numerical Simulations

These simulations were performed using COMSOL Multiphysics software, version 6.2.

4.1.1 Airflow for trapezium geometric top shaped design (case 1)

Following the Figure 4.1, airflow for the first design of the solar dryer was simulated and analyzed at different time intervals: 0 seconds, 45 seconds, 67.5 seconds, and 90 seconds. The results provide insights into the airflow patterns and their evolution over time within the dryer.

At the initial time (0 seconds, Figure 4.1a), the airflow is primarily influenced by the initial boundary conditions set for the simulation. The airflow exhibits uniform distribution, reflecting the starting state before any significant heat transfer or dynamic changes occur. By 45 seconds (Figure 4.1b), the airflow patterns start to show the impact of heat transfer and the dynamics of the air movement within the dryer. Changes in the velocity vectors and flow direction become evident as the air starts to circulate due to temperature gradients.

At 67.5 seconds (Figure 4.1c), the airflow patterns are more developed. The interaction between the heated surfaces and the cooler ambient air likely leads to more pronounced circulation patterns. This stage shows how the design facilitates or restricts airflow, indicating areas of high and low velocity.

By 90 seconds (Figure 4.1d), the airflow tends towards a steady state. The patterns observed here are critical for understanding the efficiency of the design in terms of air

circulation. Optimal airflow ensures effective heat distribution and drying efficiency, reducing hotspots and ensuring uniform drying.

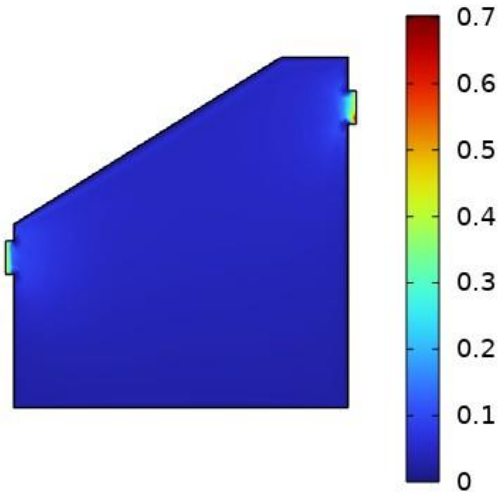

(a) Airflow at □ = 0 s

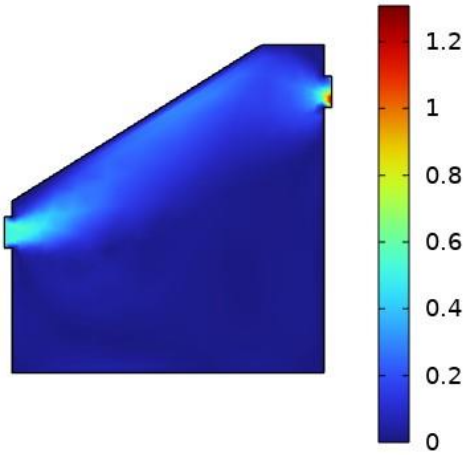

(b) Airflow at □ = 45 s

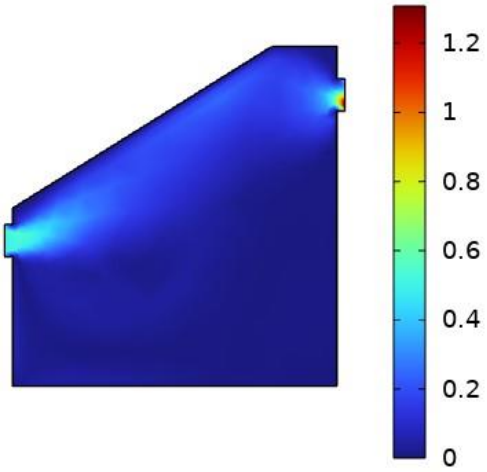

(c) Airflow at □ = 67.5 s

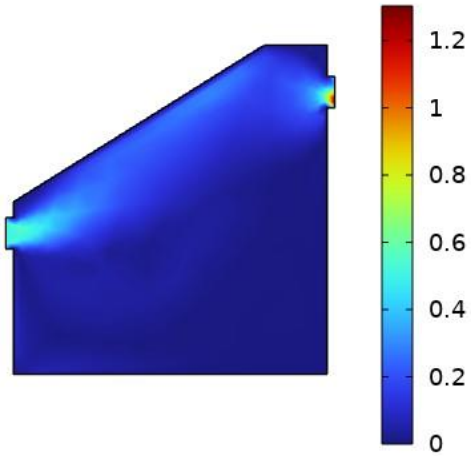

(d) Airflow at □ = 90 s

Figure 4.1: Airflow for trapezium geometric top shaped design (case 1).

4.1.2 Temperature Distribution for trapezium geometric top shaped design (case 1)

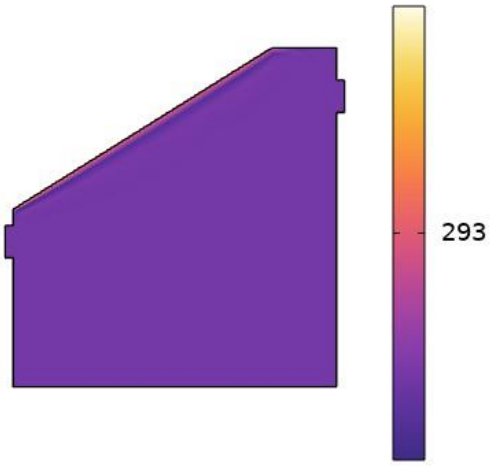

(a) Temperature distribution = 0 s

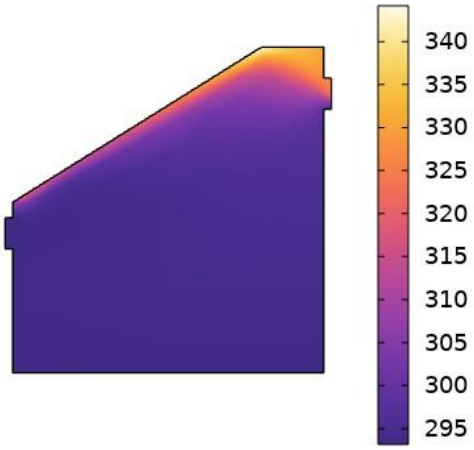

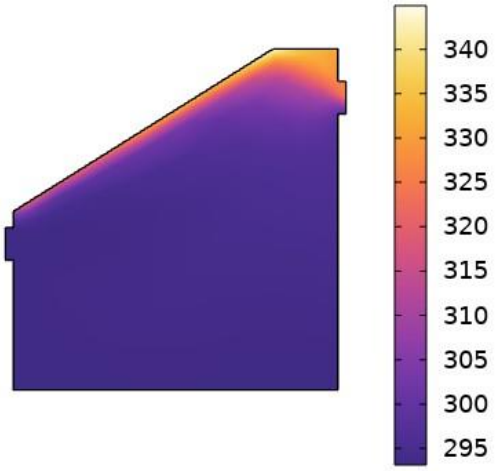

(b) Temperature distribution = 45 s

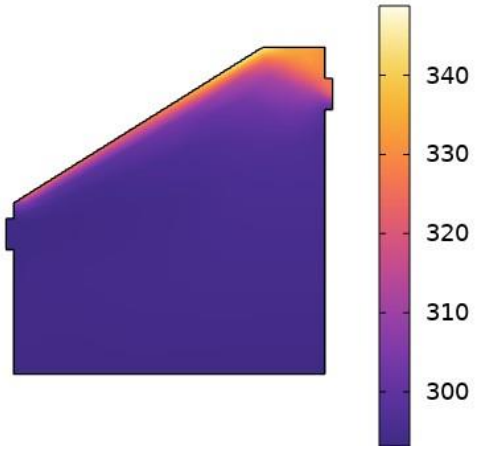

(c) Temperature distribution = 67.5 s (d) Temperature distribution = 90 s

Figure 4.2: Temperature distribution for trapezium geometric top shaped design (case 1).

The temperature distribution at different time intervals is shown in Figure 4.2 and can be summarized as follows:

At = 0s (Figure 4.2a): The initial temperature distribution is recorded at the start of the simulation. This provides a baseline for understanding how the temperature evolves over time.

At = 45s (Figure 4.2b): The temperature distribution after 45 seconds shows how the heat begins to spread within the dryer. This period often highlights the initial stages of temperature rise and the effect of solar radiation on the air inside the dryer.

At = 67.5s (Figure 4.2c): This intermediate time point provides insight into the ongoing heating process. At this stage, we can observe more pronounced temperature gradients and the movement of heat within the dryer, reflecting the dynamics of the system as it approaches a more steady state.

At = 90s (Figure 4.2d): The temperature distribution at 90 seconds shows the further progression of heating. By this time, the temperature gradients may start to stabilize,

indicating a more uniform temperature distribution or the effect of any control mechanisms within the dryer.

4.1.3 Airflow for rectangular prism geometric top shaped design (case 2)

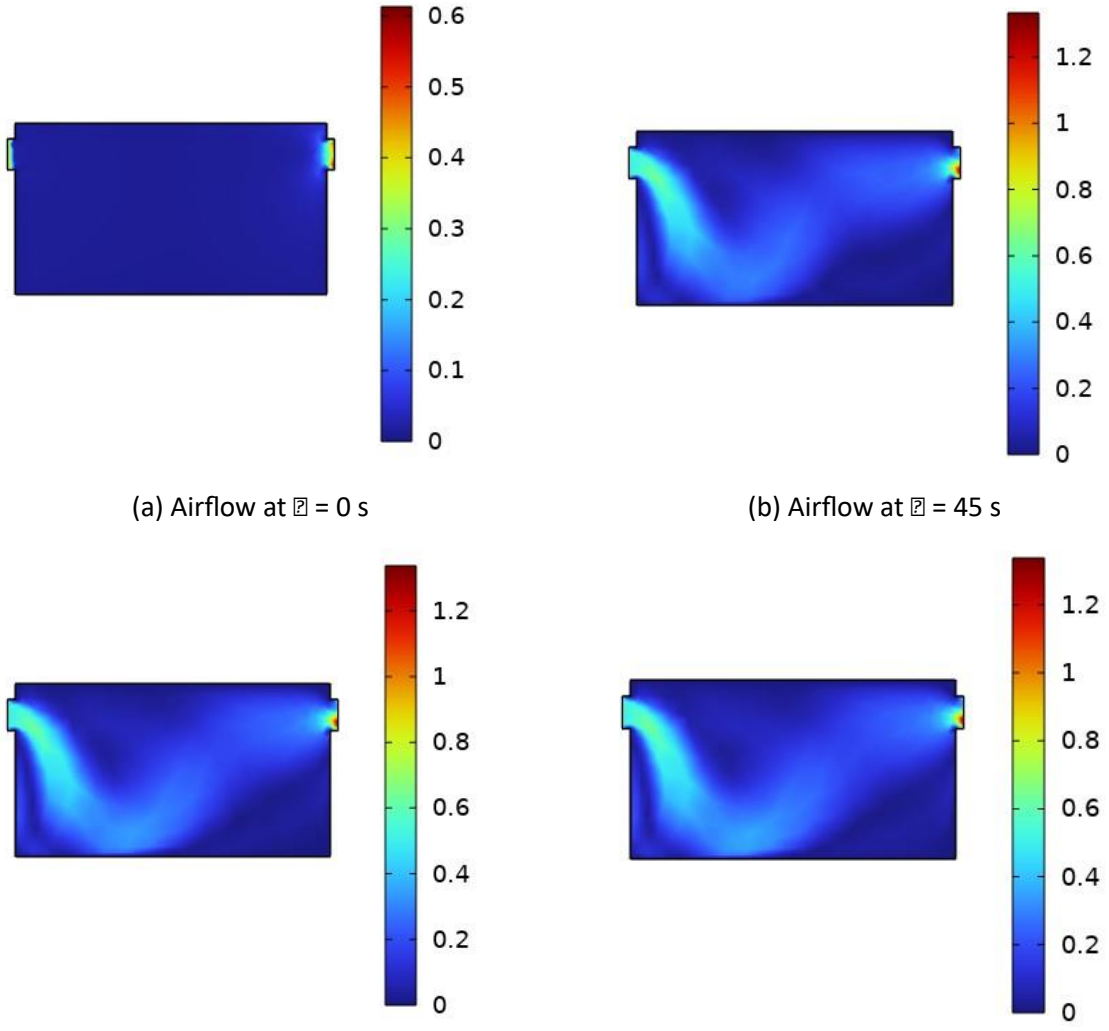

(a) Airflow at = 0 s

(b) Airflow at = 45 s

(c) Airflow at = 67.5 s

(d) Airflow at = 90 s

Figure 4.3: Airflow for rectangular prism geometric top shaped design (case 2).

The simulation results are presented at four different time intervals (Figure 4.3): Airflow at = 0 seconds (Figure 4.3a); At the initial time, the airflow distribution is at its baseline state with no significant patterns yet developed.

Airflow at = 45 seconds (Figure 4.3b); At this time, the airflow starts showing the initial development of flow patterns. There might be noticeable formation of vortices and streamlines indicating the movement of air within the dryer.

Airflow at = 67.5 seconds (Figure 4.3c); By this time, the airflow patterns are more developed. This interval might show how the air is being distributed more evenly or unevenly throughout the drying chamber.

Airflow at = 90 seconds (Figure 4.3d); At this final time interval, the airflow patterns are well-established. The simulation reveals the efficiency of air distribution in the design, indicating areas with potential dead zones (low airflow) or high-velocity zones which can impact the drying process efficiency.

4.1.4 Temperature Distribution for rectangular prism geometric top shaped design (case 2)

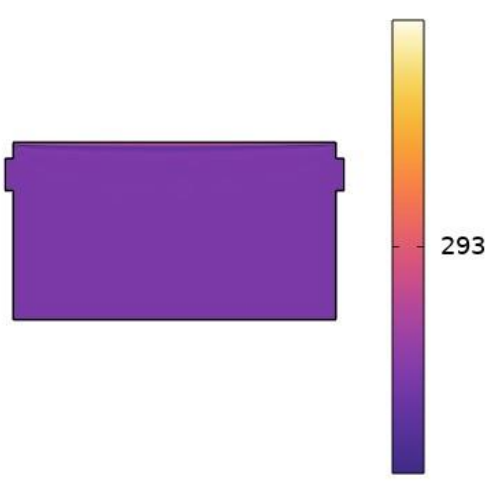

(a) Temperature distribution = 0 s

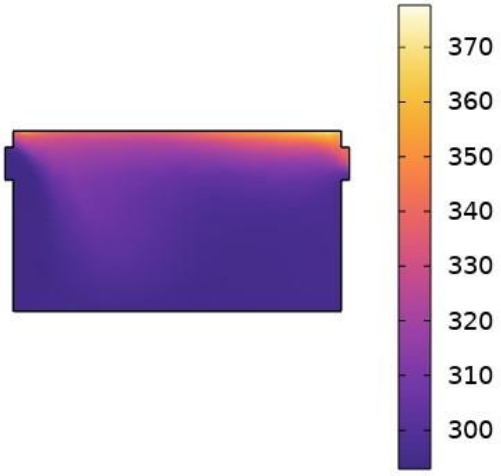

(b) Temperature distribution = 45 s

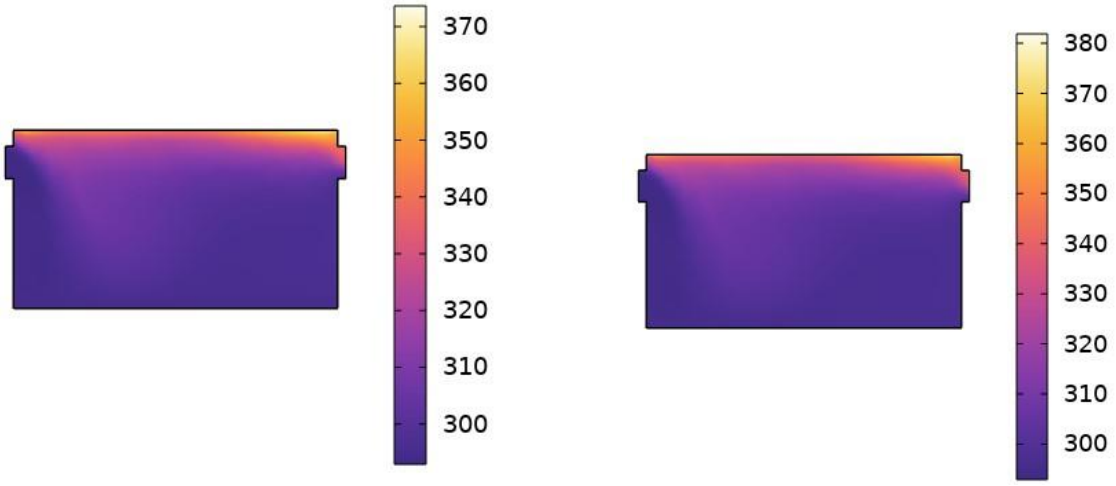

(c) Temperature distribution = 67.5 s (d) Temperature distribution = 90 s

Figure 4.4: Temperature distribution for rectangular prism geometric top shaped design (case 2).

Figure 4.4 shows the temperature distribution inside the rectangular prism geometric top-shaped solar dryer at four different time intervals: 0 seconds, 45 seconds, 67.5 seconds, and 90 seconds.

At 0 seconds (Figure 4.4a): The initial temperature distribution is uniform, indicating that the system has just started and the internal temperature is equal to the ambient conditions, around 293 K. There is no significant heat transfer at this stage.

At 45 seconds (Figure 4.4b): The temperature begins to rise as solar radiation heats the air inside the dryer. The distribution shows slight gradients, with warmer regions forming near the top of the dryer where solar energy absorption is more pronounced. The temperature increases moderately but remains fairly uniform.

At 67.5 seconds (Figure 4.4c): The temperature distribution becomes more pronounced, with noticeable gradients forming within the dryer. Warmer zones are clearly visible, indicating active heat absorption and the start of significant drying processes.

At 90 seconds (Figure 4.4d): The temperature reaches its peak in the upper sections of the dryer, suggesting that the airflow is driving heated air upwards. The gradients are more pronounced, reflecting efficient heat absorption at the top, with the temperature ranging around 294 K.

4.1.5 Airflow for triangular prism geometric top shaped design (case 3)

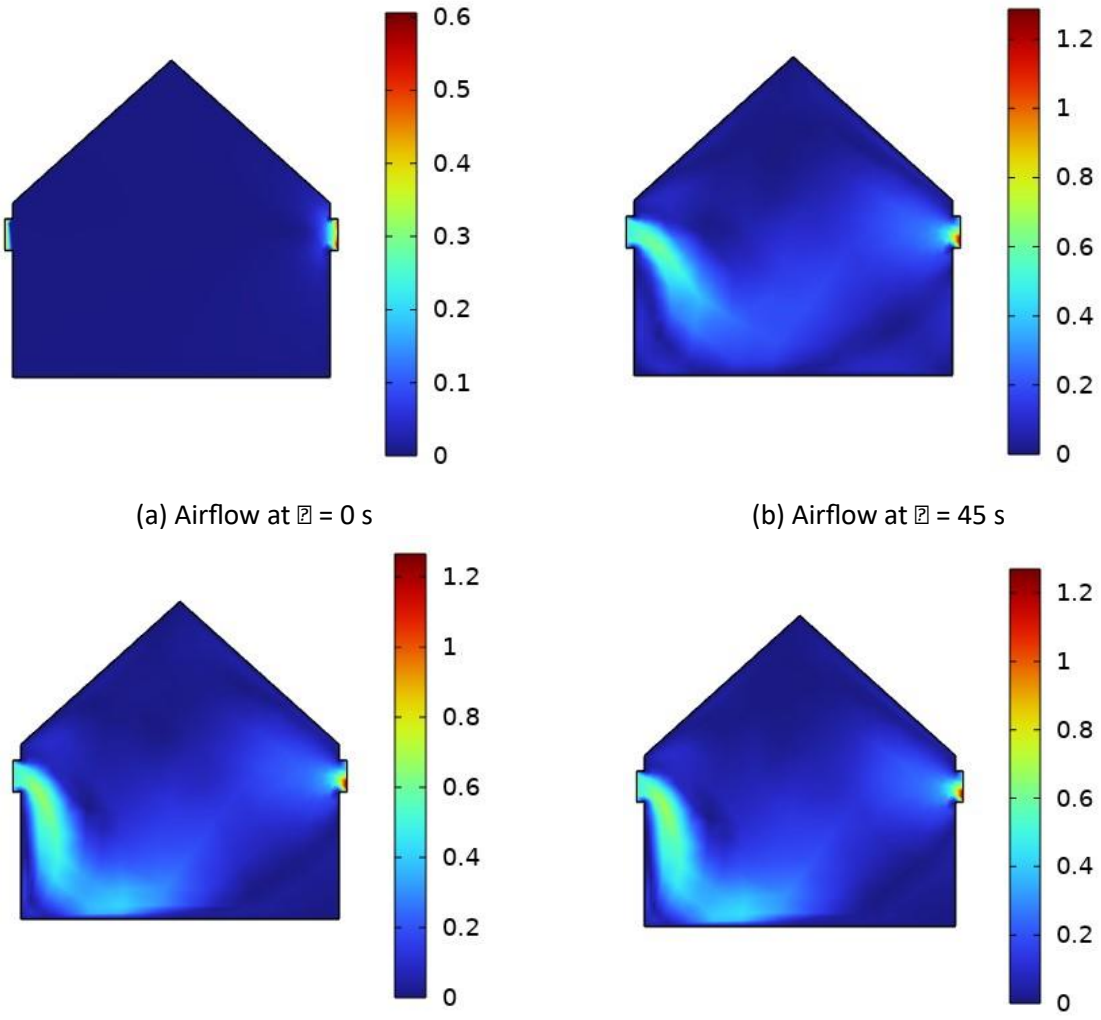

(a) Airflow at □ = 0 s

(b) Airflow at □ = 45 s

(c) Airflow at □ = 67.5 s

(d) Airflow at □ = 90 s

Figure 4.5: Airflow for triangular prism geometric top shaped design (case 3).

The simulation results for the airflow in the third design of the solar dryer provide insightful observations over time, depicted at four specific time intervals: □ = 0 s, □ = 45 s, □ = 67.5 s, and □ = 90 s.

At the initial time □ = 0 s, the airflow distribution shows a uniform pattern as the air enters the dryer. This uniformity indicates that the initial conditions set for the simulation

were stable and effectively initiated the airflow process. As time progresses to = 45 s, the airflow begins to exhibit more distinct patterns. The air movement starts to form streams and vortices, indicating the influence of the dryer's structural design on airflow dynamics. These patterns become more pronounced, suggesting the dryer's internal architecture plays a crucial role in directing the air.

By = 67.5 s, the airflow within the dryer continues to evolve, showing further development of streams and turbulence. This stage is critical as it highlights areas within the dryer where airflow might be more concentrated, potentially impacting the drying efficiency in these regions. The formation of vortices and streams suggests that the airflow is reaching a more complex and stabilized pattern influenced by the dryer's design.

Finally, at = 90 s, the airflow reaches a quasi-steady state where the patterns observed are likely to be maintained with minor fluctuations. The established airflow streams and vortices indicate areas where the air velocity is higher, which can correlate with more efficient drying zones within the solar dryer. This steady-state behavior is essential for predicting the long-term performance of the dryer and for identifying potential areas for design optimization to improve overall drying efficiency.

4.1.6 Temperature Distribution for triangular prism geometric top shaped design (case 3)

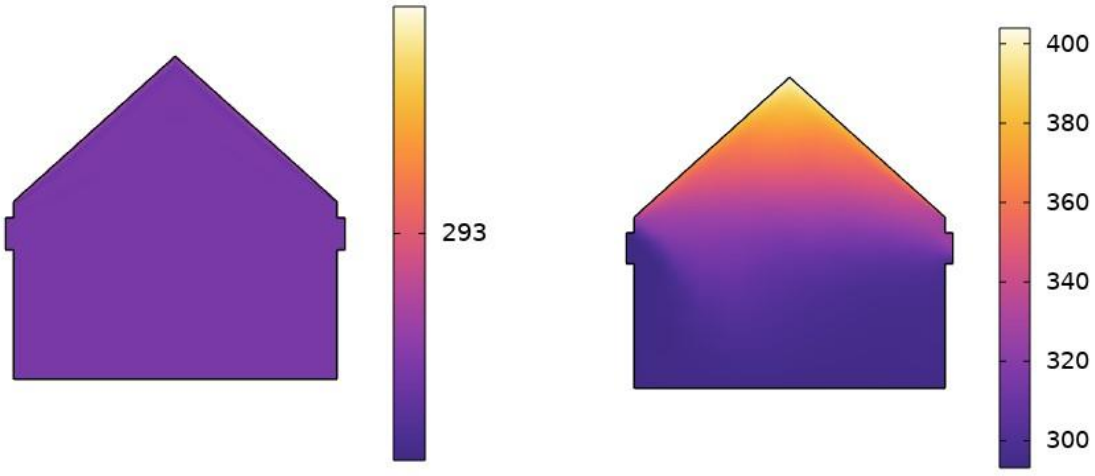

(a) Temperature distribution = 0 s

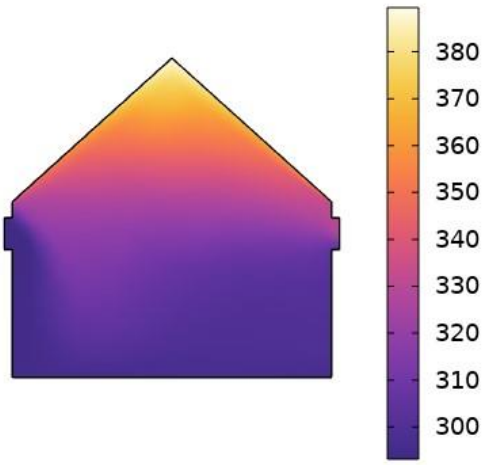

(b) Temperature distribution = 45 s

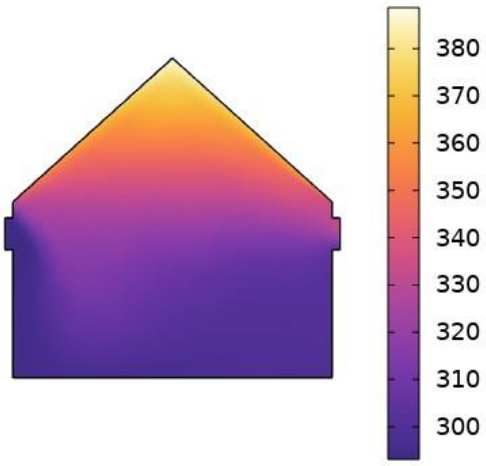

(c) Temperature distribution = 67.5 s

(d) Temperature distribution = 90 s

Figure 4.6: Temperature distribution for triangular prism geometric top shaped design (case 3).

In Figure 4.6, the temperature distribution for the triangular prism geometric top-shaped solar dryer is displayed at four different time intervals: 0 seconds, 45 seconds, 67.5 seconds, and 90 seconds. The temperature distribution evolves as follows:

At t = 0 seconds: The initial temperature is nearly uniform across the drying chamber, reflecting ambient conditions before significant heat transfer begins.

At t = 45 seconds: The temperature within the dryer begins to rise, with heat primarily concentrated near the heated surfaces. A gradient starts to form, indicating the initial absorption of solar energy.

At t = 67.5 seconds: The temperature continues to increase, and more distinct temperature zones appear within the dryer. Warmer areas emerge near the air inlet and heated regions, while cooler zones remain farther from the heat sources.

At t = 90 seconds: The temperature stabilizes with a more uniform distribution throughout the chamber, although higher temperatures are still observed near heat

entry points. The gradual equalization of temperature suggests that the airflow within the dryer is distributing heat more evenly as the system approaches a quasi-steady state.

4.2 Graphical Results

The analysis of the solar dryers was focused on one point located in the left hand side of the different dryers, here referred to as **point 1** and a second point located in the right hand side of the different dryers, here referred to as **point 2**. Figure 4.7 above illustrates the graph for the variation of temperature over time at a specific point inside a direct solar dryer (left lower end). The x-axis represents time in seconds, ranging from 0 to 90 seconds, while the y-axis shows the temperature in Kelvin, spanning from 293.14 K to approximately 293.52 K. Initially, the temperature remains relatively stable at around 293.16 K for the first 40 seconds, indicating a period of minimal temperature change. This steady state could be attributed to the time required for the dryer to overcome initial thermal inertia or the effect of an initial equilibrium condition inside the dryer.

As time progresses beyond 40 seconds, there is a noticeable increase in temperature, which becomes more pronounced after the 60-second mark. This phase represents a period of

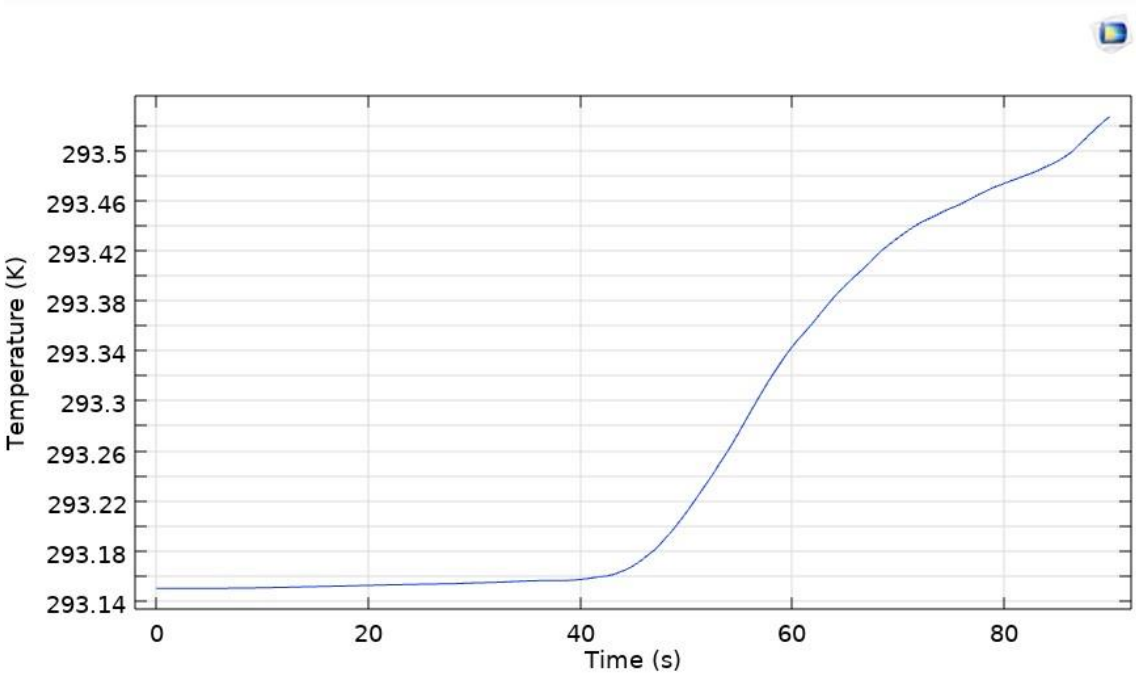

Figure 4.7: Graph showing temperature variation at point 1 in case 1

active heating, where the temperature rises significantly from about 293.18 K to 293.52 K by the 80-second mark. The curve's upward slope indicates a consistent rate of temperature increase, likely due to the intensified absorption of solar energy as the system reaches a more effective operational state. This pattern suggests that the direct solar dryer begins to efficiently convert solar energy into heat, thus raising the temperature at the measured point within the dryer.

Figure 4.8 above illustrates the graph for the variation of temperature over time for a specific point inside a direct solar dryer ((right lower end)). The x-axis represents time in seconds, ranging from 0 to 85 seconds, while the y-axis denotes temperature in Kelvin, spanning from approximately 293.15 K to 293.6 K. The temperature shows an initial stability around 293.15 K for the first 10 seconds, followed by a gradual increase. Around the 20-second mark, there is a notable rise in temperature, reaching around 293.25 K, before a slight plateau and subsequent decline.

After the initial fluctuations, a more consistent increase is observed from around the

40-second mark, with the temperature climbing steadily towards 293.6 K by the end of the

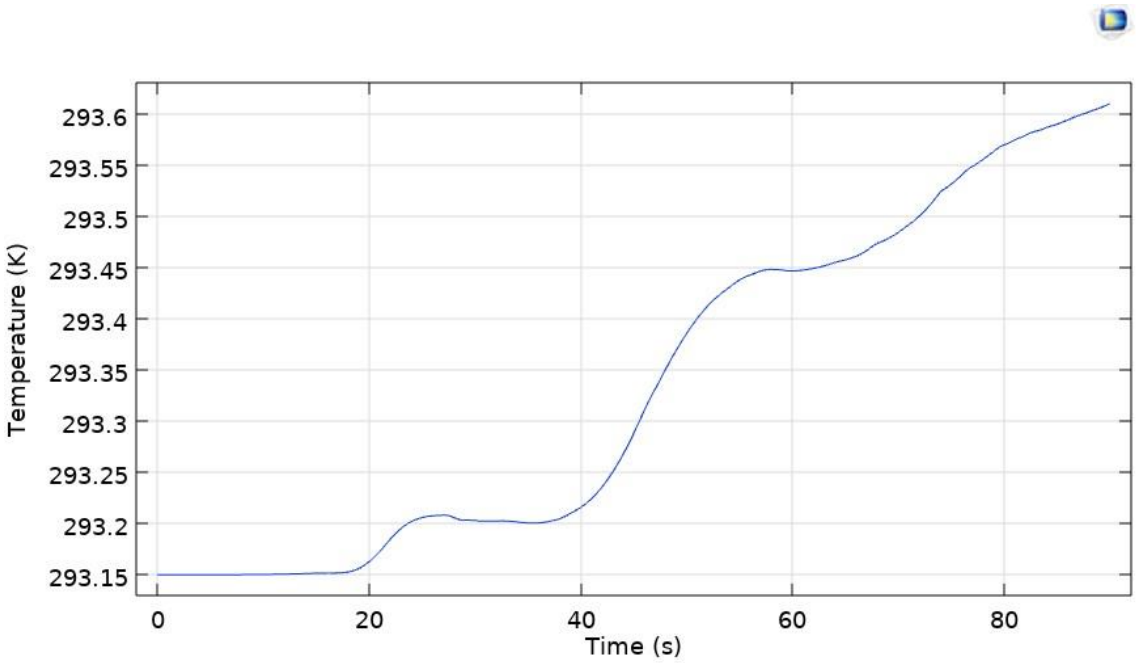

Figure 4.8: Graph showing temperature variation at point 2 in case 1

observed period. This trend indicates that the direct solar dryer gradually increases the temperature at the measured point, with minor oscillations possibly due to intermittent solar exposure or internal adjustments within the dryer. The overall upward trend suggests a sustained heating process facilitated by the direct solar drying mechanism.

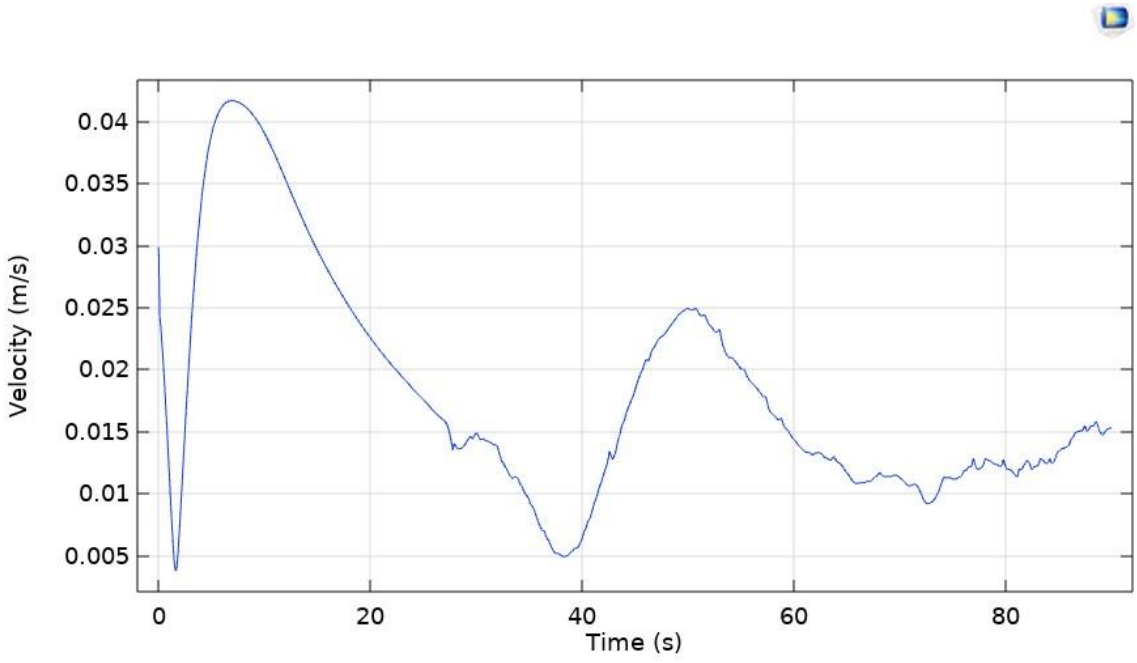

Figure 4.9: Graph showing velocity variation at point 1 in case 1

Figure 4.9 above illustrates the graph for the variation of velocity over time for a specific point within a direct solar dryer. Initially, the velocity experiences a rapid increase, peaking at approximately 0.04 m/s within the first few seconds. This sharp rise suggests a sudden influx of air, possibly due to the initial heating and expansion of air inside the solar dryer. Following this peak, the velocity declines steadily, reaching a low point around 0.005 m/s at about 20 seconds. This decline might be attributed to the stabilization of airmovementastheinitialsurgedissipatesandthesystembeginstoreachamoresteadystate.

Astimeprogresses,thevelocityundergoesfurtherfluctuations,indicatingvaryingconditions within the solar dryer. Around the 40-second mark, the velocity increases again, reaching another peak just below 0.03 m/s, before decreasing once more. This pattern of rising and falling velocity continues throughout the observed period, suggesting periodic changes in the drying conditions, possibly due to intermittent solar radiation, changes in temperature, or other environmental factors. The graph in Figure 4.9 reflects a dynamic system with ongoing adjustments in air velocity, crucial for the efficient drying process inside the solar dryer.

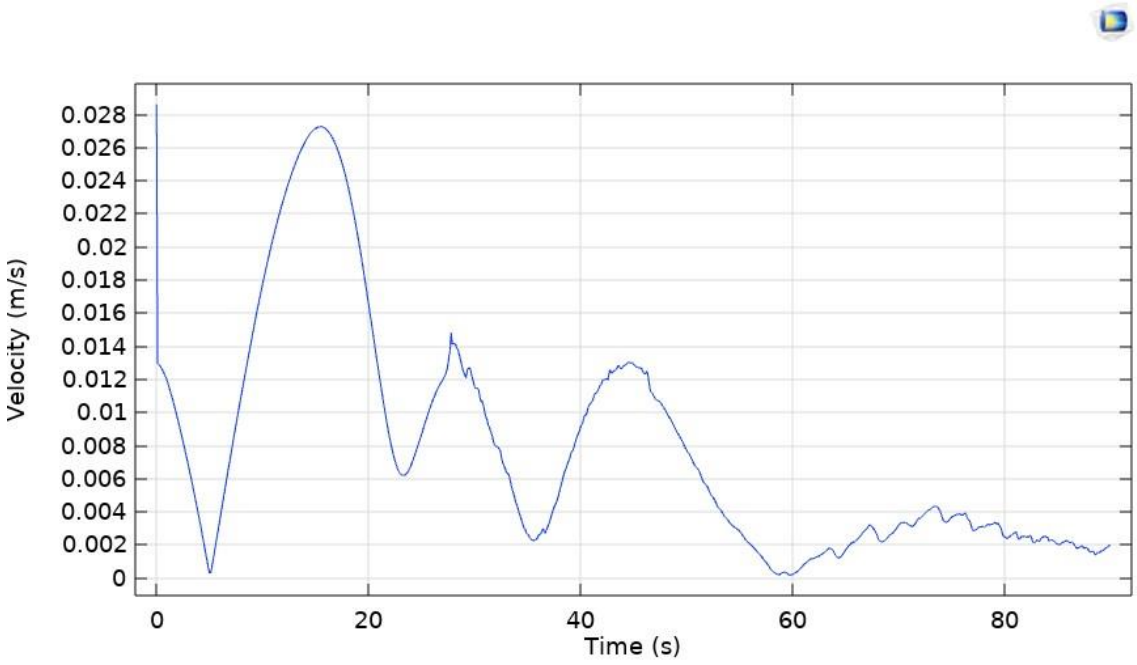

Figure 4.10: Graph showing velocity variation at point 2 in case 1

The graph in Figure 4.10 depicts the variations in velocity at a particular point inside a direct solar dryer over a period of approximately 90 seconds. Initially, the velocity exhibits a sharp spike, reaching a peak of about 0.028 m/s. This is followed by a rapid decline to nearly 0.006 m/s within the first 10 seconds. Subsequently, the velocity undergoes several oscillations, with prominent peaks and troughs. The first major peak occurs around 15 seconds, where the velocity again reaches approximately 0.026 m/s, followed by a trough at around 25 seconds where the velocity dips below 0.008 m/s.

As time progresses, these oscillations become less pronounced, indicating a gradual stabilization of the velocity. Between 40 to 60 seconds, the velocity fluctuations become smaller, with peaks reaching around 0.014 m/s and troughs near 0.006 m/s. Beyond 60 seconds, the velocity continues to decrease and oscillate with smaller amplitudes, eventually settling around 0.004 m/s by the 90-second mark. This pattern suggests an initial period of instability followed by a gradual stabilization as the system within the solar dryer reaches equilibrium.

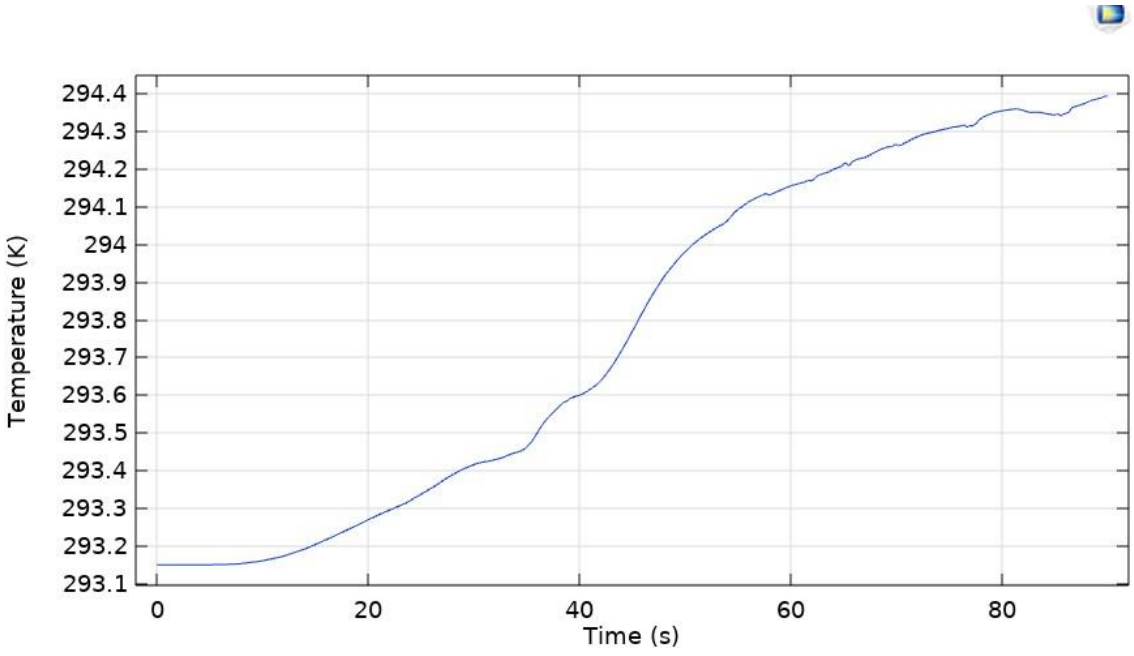

Figure 4.11: Graph showing temperature variation at point 1 in case 2

Figure 4.11 above illustrates the graph for the variation of temperature distribution at a specific point within a direct solar dryer over a period of approximately 90 seconds. Initially, the temperature at this point is relatively low, around 293.1 K, which suggests that the system has just been exposed to the sunlight or that the solar dryer is starting up. As time progresses, the temperature begins to rise gradually, reflecting the initial absorption of solar energy. This gradual increase continues until about 20 seconds, where the temperature reaches around 293.5 K. This phase indicates the initial heating period where the solar energy is being uniformly distributed within the dryer.

Between 20 to 40 seconds, there is a noticeable steep increase in temperature, reaching up to around 294 K. This rapid rise could be due to the dryer reaching a more optimal angle or orientation towards the sun, thereby increasing the efficiency of solar energy absorption. After this steep rise, the temperature continues to increase but at a more moderate and consistent rate, indicating a stable phase where the dryer maintains a relatively uniform temperature distribution. Minor fluctuations observed in the latter part of the graph might be attributed to variations in solar intensity or airflow within the dryer. Overall, the graph suggests that the direct solar dryer effectively harnesses solar energy to increase and maintain the temperature at a specific point, which is crucial for efficient drying processes. Figure 4.12 above illustrates the graph for the variation of

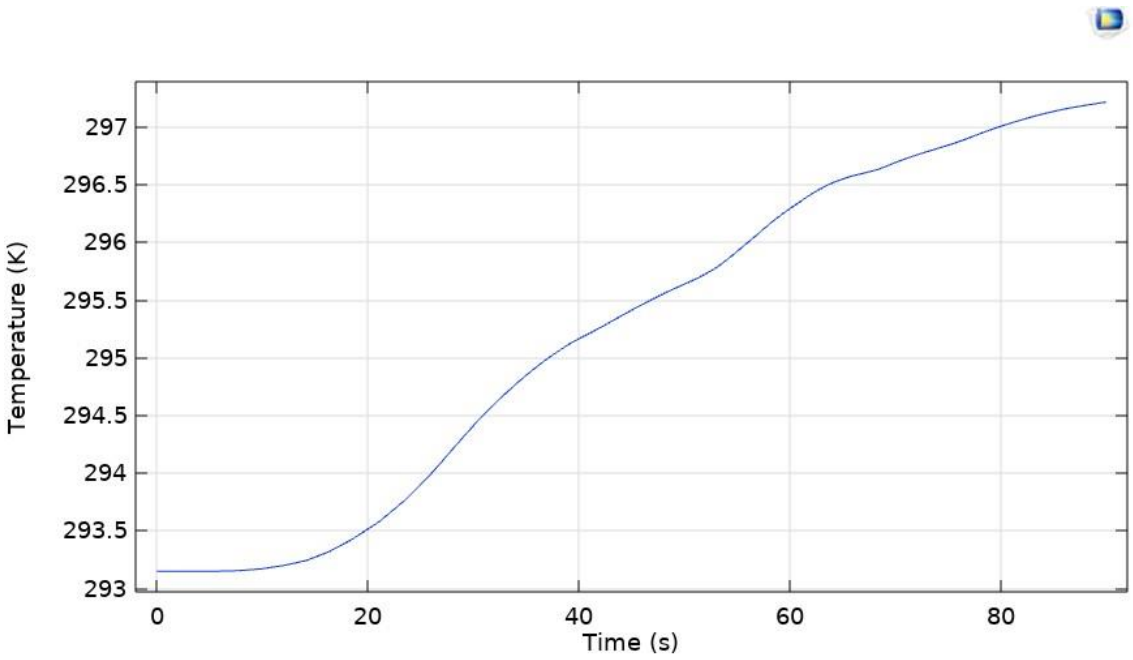

Figure 4.12: Graph showing temperature variation at point 2 in case 2

temperature distribution at a specific point within a direct solar dryer over a period of time. The temperature is measured in Kelvin (K) and plotted against time in seconds (s). Initially, the temperature remains constant at approximately 293 K, indicating a stable starting condition. After about 10 seconds, the temperature begins to increase gradually. This rise in temperature continues steadily throughout the duration of the measurement, reflecting the influenceof solar energybeing absorbedandconvertedtoheatwithin thedryer.

As time progresses, the temperature shows a smooth and consistent increase, reaching just below 298 K by the end of the 90-second period. The curve suggests a typical response of the drying system to solar radiation, where the temperature rises as the dryer absorbs more heat from the sunlight. The absence of sudden spikes or drops in the temperature curve indicates a uniform distribution of heat and efficient energy absorption within the solar dryer. This behavior is essential for optimizing the drying process, ensuring that the material being dried receives consistent and adequate heat throughout the operation.

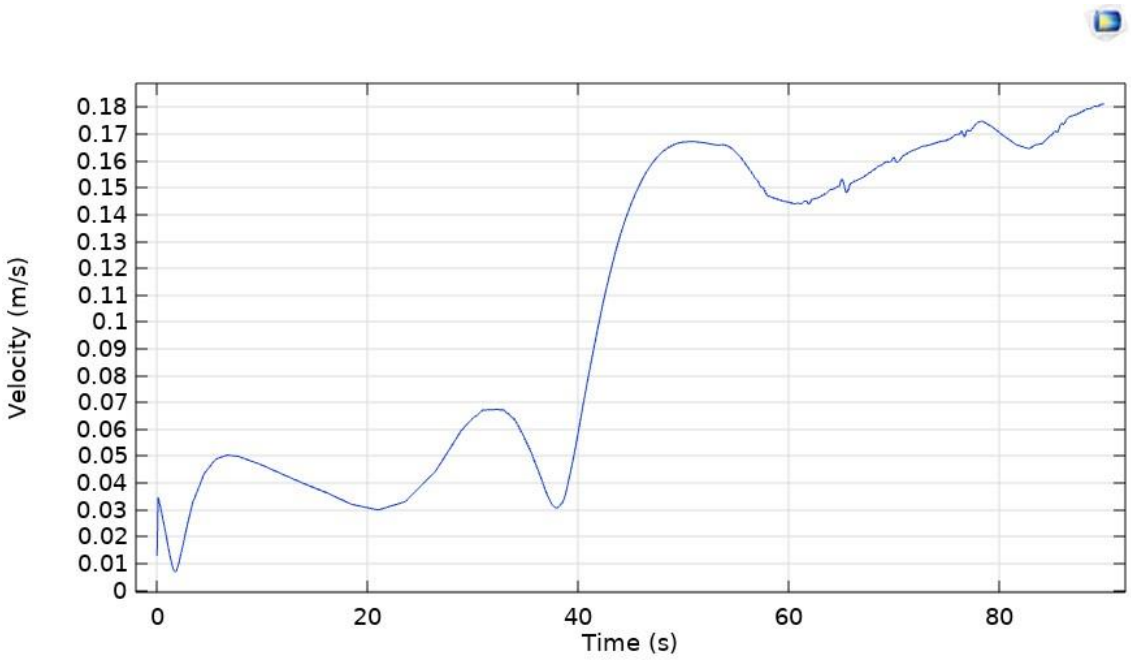

Figure 4.13: Graph showing velocity variation at point 1 in case 2

Figure 4.13 above illustrates the graph for the velocity variation of air within a direct solar dryer over a span of 90 seconds. The x-axis represents time in seconds, while the y-axis denotes the velocity in meters per second (m/s). The data illustrates a fluctuating velocity pattern, indicative of dynamic changes in air movement within the dryer system. Initially, the velocity experiences a sharp increase, reaching approximately 0.03 m/s within the first 10 seconds. This is followed by a slight dip and subsequent oscillations, with peaks and troughs indicating periodic accelerations and decelerations of the airflow.

As time progresses, a notable spike occurs around the 35-second mark, where the velocity rapidly escalates to about 0.17 m/s, the highest point recorded in the graph in Figure 4.13. Following this peak, there is a significant drop, after which the velocity stabilizes somewhat but continues to exhibit smaller fluctuations. These variations likely correspond to the influence of solar radiation, changes in air temperature, and potential obstructions or modifications within the dryer. The overall trend suggests that while there are periods of relative stability, the air velocity in the direct solar dryer is subject

to considerable variability, reflecting the complex interplay of factors affecting airflow in such systems.

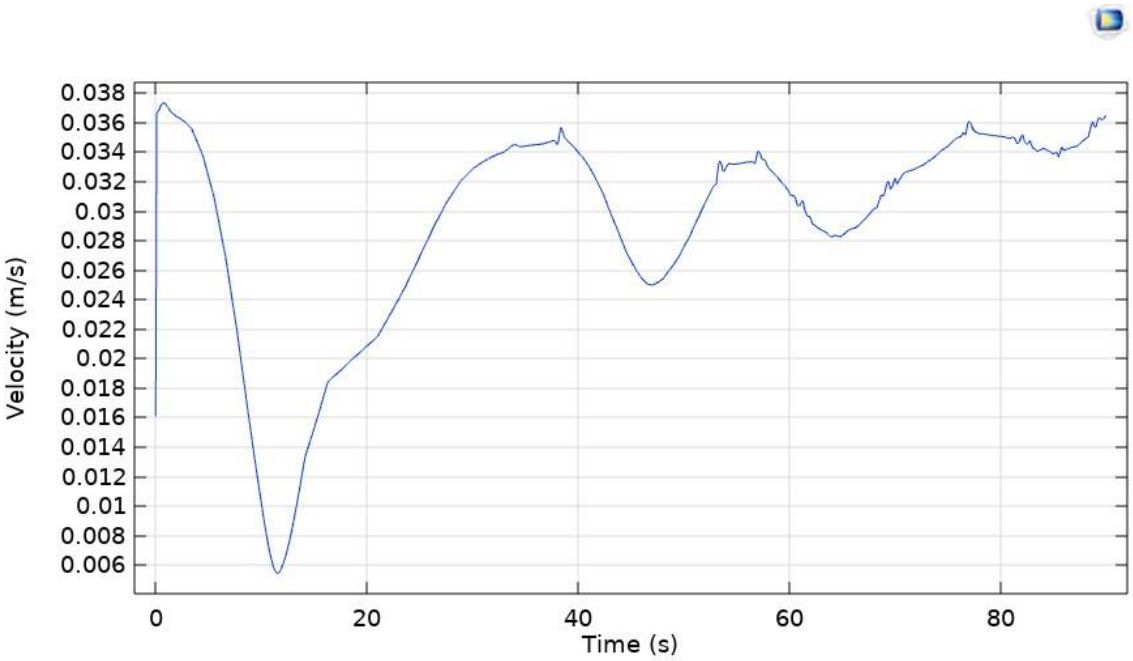

Figure 4.14: Graph showing velocity variation at point 2 in case 2

Figure 4.14 above illustrates the graph for the variation of velocity at a specific point within a direct solar dryer over a time span of 90 seconds. Initially, the velocity is relatively high, peaking just below 0.038 m/s, but it quickly drops to a low of approximately 0.006 m/s around the 10-second mark. This significant decrease in velocity is followed by a gradual recovery, with the velocity increasing steadily until it reaches about 0.028 m/s at around 35 seconds.

From this point, the velocity experiences another decrease, though less steep than the initial drop, reaching a minimum of approximately 0.018 m/s at around 55 seconds. Following this dip, there is a relatively smooth increase in velocity, with minor fluctuations, until it stabilizes near 0.034 m/s towards the end of the observed period. Overall, the graph indicates a cyclical pattern of velocity changes, characterized by sharp declines and gradual recoveries, suggesting variations in the air flow or thermal dynamics within the solar dryer.

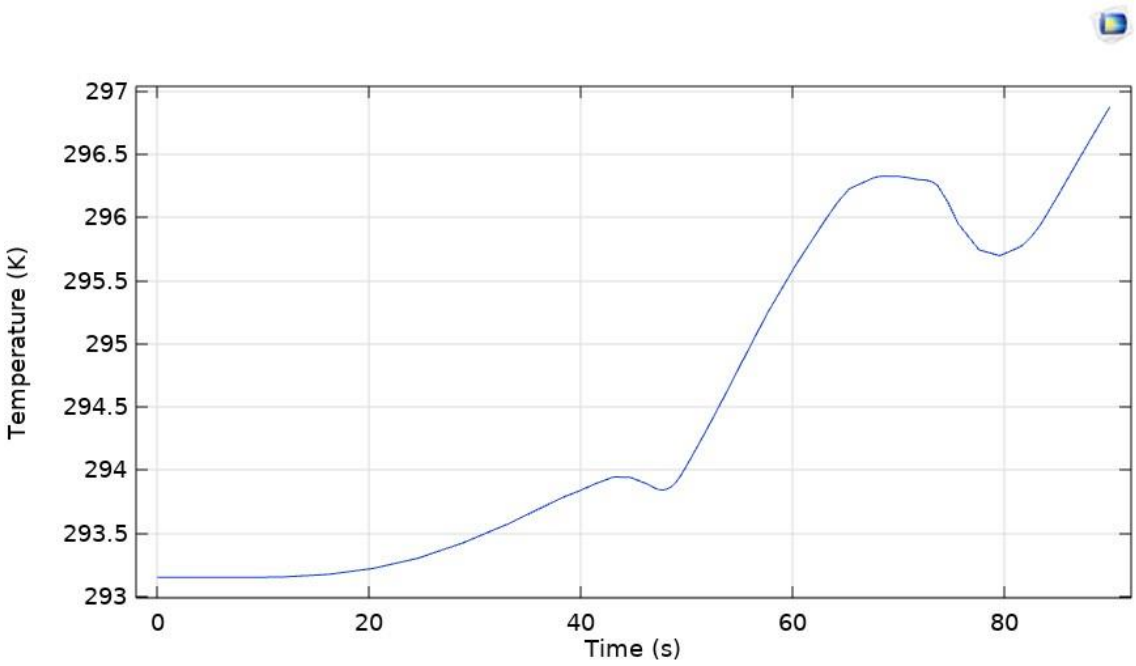

Figure 4.15: Graph showing temperature variation at point 1 in case 3

Figure 4.15 above depicts the graph for the variation of temperature over time at a specific point inside a direct solar dryer. Initially, the temperature starts at approximately 293.5 K and remains fairly constant for the first 20 seconds. This indicates that the system is likely in a stable state before any significant solar heating effect takes place. After this period, the temperature begins to rise gradually, reflecting the onset of solar radiation impacting the drying process. Between 20 and 40 seconds, a slight increase in temperature is observed, suggesting a modest accumulation of thermal energy.

From around 40 seconds onward, there is a more pronounced increase in temperature, peaking just below 297 K at approximately 70 seconds. This steep rise suggests an intense phase of solar heating. After reaching this peak, a slight dip occurs around the 75-second mark, indicating a temporary decrease in thermal energy absorption or possibly an increase in heat loss. Subsequently, the temperature resumes its upward trend, reaching around 297 K by the 85-second mark. This overall trend showcases the dynamic nature

of temperature changes within the direct solar dryer, driven primarily by the variations in solar radiation intensity and the system's thermal response.

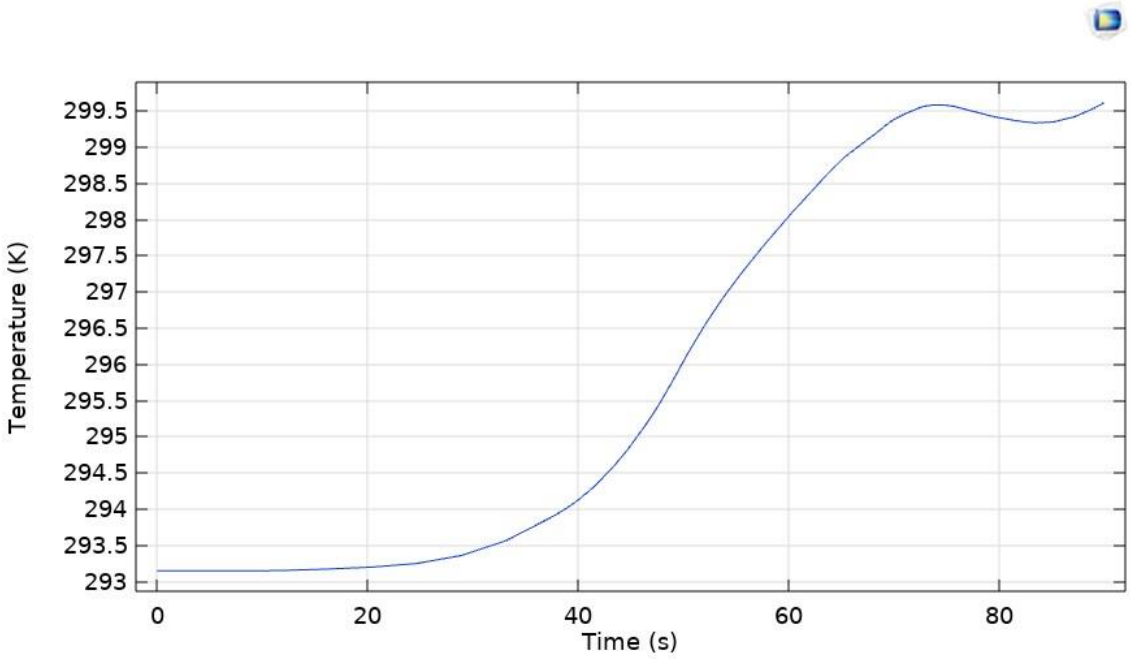

Figure 4.16: Graph showing temperature variation at point 2 in case 3

Figure 4.16 above illustrates the graph for the variation of temperature (in Kelvin) with respect to time (in seconds) at a specific point inside a direct solar dryer. At the beginning of the observation period, the temperature remains relatively constant at approximately 293 K for the first 20 seconds. This indicates a period where the point inside the solar dryer has not yet started to absorb significant heat from the solar radiation. After this initial steady phase, there is a noticeable increase in temperature, suggesting that the point has started to absorb heat.

Fromaround20secondsto60seconds, thetemperaturerisessharply, reachingapproximately 299 K. This sharp increase indicates a significant absorption of heat due to direct solar radiation, leading to a rapid rise in temperature at the measured point. After 60 seconds, the rate of temperature increase slows down, and the graph shows a slight decline before stabilizing around 299.5 K. This stabilization suggests that the point inside the solar dryer has reached a thermal equilibrium where the rate of heat

absorption is balanced by the rate of heat loss, maintaining a relatively constant temperature towards the end of the observation period.

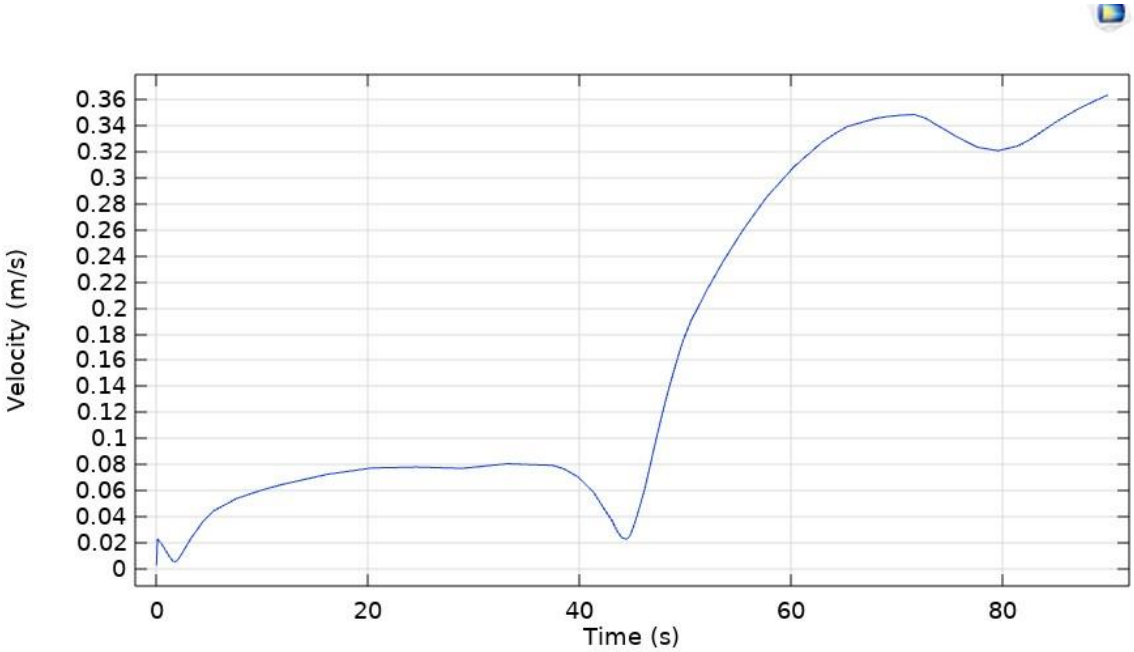

Figure 4.17: Graph showing velocity variation at point 1 in case 3

Figure 4.17 above illustrates the graph for the variation of velocity over time at a specific point within a direct solar dryer. The velocity is measured in meters per second (m/s), and the time is in seconds (s). Initially, the velocity starts at a low value of approximately 0.02 m/s and shows slight fluctuations for the first 20 seconds. There is a small dip in velocity around the 10-second mark, indicating a brief reduction in airflow speed at that particular point inside the solar dryer.

After the initial fluctuations, the velocity maintains a relatively steady value around 0.06 m/s until about the 40-second mark, where a noticeable drop occurs, bringing the velocity down to nearly 0.02 m/s again. Following this dip, there is a significant increase in velocity, peaking at around 0.36 m/s by the 65-second mark. This peak is followed by a minor decrease, then a subsequent rise, suggesting variations in the drying conditions or external influences on the solar dryer. Overall, the graph highlights the dynamic nature

of airflow within the solar dryer, with notable fluctuations and trends over the observed period.

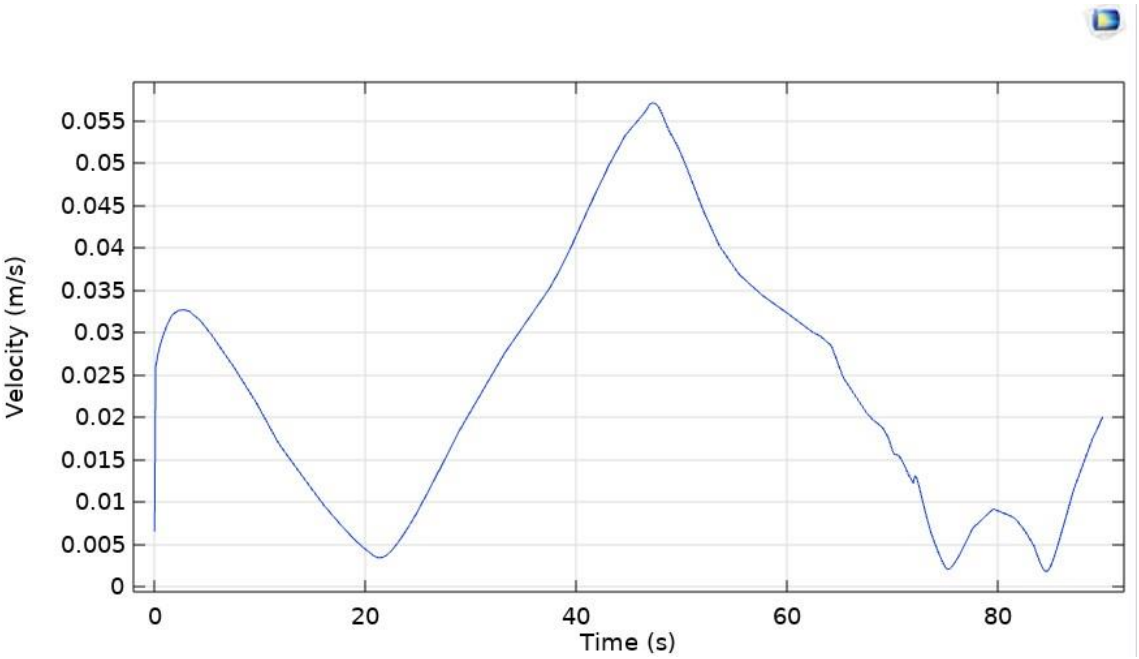

Figure 4.18: Graph showing velocity variation at point 2 in case 3

Figure 4.18 above illustrates the graph for the variation of velocity over time for a specific point inside a direct solar dryer. The horizontal axis represents time in seconds, ranging from 0 to 90 seconds, while the vertical axis represents velocity in meters per second (m/s), ranging from 0 to 0.055 m/s. Initially, there is a noticeable spike in velocity, peaking around 0.033 m/s within the first few seconds. This rapid increase is followed by a decline, reaching a minimum velocity of approximately 0.003 m/s around the 20-second mark.

As time progresses, the velocity experiences another substantial increase, peaking at about 0.055 m/s around the 40-second mark, which is the highest velocity recorded in the given time frame. After this peak, there is a gradual decline in velocity, with a minor dip around 60 seconds before another small peak and subsequent decline, reaching a low point near 0.007 m/s around 80 seconds. Towards the end of the graph, there is a slight increase in velocity, suggesting ongoing fluctuations. These variations in velocity

could be attributed to the changes in solar radiation, airflow dynamics, or other environmental factors influencing the drying process within the solar dryer.

4.2.1 Discussion of results

4.2.1.1 Temperature variation analysis for first design of the solar dryer

The investigation of temperature distribution inside the first design of the direct solar dryer, as illustrated by the two graphs in Figures 4.7 and 4.8, reveals non-uniform heating dynamics at different points (left and right lower ends respectively) within the dryer. Graph in Figure 4.7 shows a delayed but steady temperature increase starting at around 40 seconds, reaching a peak of approximately 293.5 K. In contrast, Graph in Figure 4.8 indicates an earlier rise in temperature at around 20 seconds, followed by a brief plateau and another increase after 40 seconds, peaking slightly higher at 293.6 K. These differences suggest that the temperature distribution varies significantly within the dryer, likely due to factors such as variations in solar radiation exposure, airflow, or material properties.

A more uniform drying process is generally indicated by a smoother and more consistent temperature increase, without sudden spikes or plateaus. In this context, graph in Figure 4.7 shows a more gradual and steady increase in temperature after the initial delay, without significant fluctuations, which suggests a more uniform heating process. In contrast, graph in Figure 4.8 displays a more complex pattern with two distinct periods of temperature rise and a brief plateau, indicating less uniformity in the temperature distribution.

4.2.1.2 Temperature variation analysis for second design of the solar dryer

The two graphs in Figures (4.11 and 4.12) illustrate the temperature distribution at different points (left and right lower ends respectively) within the second design of the direct solar dryer over time. Graph in Figure 4.11 shows a temperature range from approximately 293.1 K to 294.4 K over a period of 90 seconds, with noticeable

fluctuations and an overall upward trend. Graph in Figure 4.12 indicates a broader temperature range from around 293 K to 297 K within the same time frame, exhibiting a smoother and more consistent increase in temperature. This comparison suggests that the second measurement point (right lower end) experiences a more substantial and stable rise in temperature compared to the first (left lower end), possibly due to variations in solar exposure or the position within

the dryer.

It is observed that graph in Figure 4.12 indicates better uniform drying. This conclusion is based on the smoother and more consistent increase in temperature observed in the graph in Figure 4.12. Uniform and stable temperature rise is crucial for efficient and consistent drying, as it ensures that the drying process is evenly distributed across the material being dried. In contrast, graph in Figure 4.11 shows more fluctuations, suggesting less uniform heating which can lead to uneven drying.

4.2.1.3 Temperature variation analysis for third design of the solar dryer

Graphs in Figures (4.15, 4.16) display the temperature distribution inside the third design of a direct solar dryer at different points (left and right lower ends respectively) over time. Graph in Figure 4.15 shows the temperature changes at a point at the left lower end, starting at approximately 293 K and fluctuating between 293 K and nearly 297 K over the period of 90 seconds. The temperature exhibits several minor fluctuations but generally trends upward. Graph in Figure 4.16 depicts the temperature at a point at the right lower end, also starting at around 293 K but rising more steadily and peaking at around 299 K before slightly decreasing towards the end. This comparison indicates that the point at the right lower end experiences a more consistent and higher overall temperature increase compared to the point at the left lower end, suggesting a variation in heat distribution within the dryer, potentially due to differences in solar exposure or airflow dynamics.

Graph in Figure 4.16, which shows the temperature changes at the point at the right lower end of the dryer, indicates better uniform drying. The temperature in this graph rises steadily and reaches a higher, more stable peak around 299 K before slightly decreasing towards the end. This steady increase and higher temperature suggest a more consistent and effective drying process. In contrast, graph in Figure 4.15 exhibits more fluctuations and lower overall temperatures, indicating less uniform drying conditions.

4.2.1.4 Velocity variation analysis for first design of the solar dryer

Graphs in Figures (4.9 and 4.10) display the velocity variation inside the first design of a direct solar dryer at different points (left and right lower ends respectively) over time. Graph in Figure 4.9 shows a higher initial peak velocity of around 0.04 m/s, followed by a gradual decline with minor fluctuations, indicating variations in airflow dynamics at that particular location. Graph in Figure 4.10 has a lower initial peak velocity of approximately 0.028 m/s and also exhibits a pattern of decay with fluctuations. The velocity trends in both graphs suggest that airflow behavior inside the dryer is not uniform and varies significantly across different points, likely influenced by factors such as dryer design, air inlet and outlet positions, and the distribution of solar energy.
Graph in Figure 4.10 indicates better uniform drying within the direct solar dryer. This is evidenced by its lower initial peak velocity of around 0.028 m/s compared to the peak of 0.04 m/s for Graph in Figure 4.9, and by its smaller fluctuations over time. Graph in Figure 4.10 stabilizes more towards the end, indicating a more consistent airflow. Consistent airflow is critical for uniform drying, as it ensures that all areas within the dryer receive a similar amount of air movement and heat, leading to more even drying of the contents. Therefore, graph in Figure 4.10 suggests a more uniform drying process, implying that the airflow at the right lower end of the dryer facilitates uniform drying.

4.2.1.5 Velocity variation analysis for second design of the solar dryer

In the investigation of velocity distribution inside the second design of a direct solar dryer, the two provided graphs in Figures (4.13 and 4.14) illustrate the temporal

variations in velocity at two distinct points (left and right lower ends respectively) within the dryer. Graph in Figure 4.13 shows a more pronounced and fluctuating increase in velocity, peaking at around 0.18 m/s before gradually stabilizing. This indicates significant dynamic changes and possibly not laminar airflow patterns at this point. In contrast, graph in Figure 4.14 reveals a more moderate and less variable velocity distribution, with a maximum velocity of approximately 0.038 m/s and a more consistent trend over time. The differences between these two graphs in Figures (4.13 and 4.14) suggest varying airflow characteristics within different regions of the dryer, likely influenced by the geometry and design of the dryer, as well as the positioning of the heat source and vents. Graph in Figure 4.14 indicates better uniform drying. This graph shows a more moderate and consistent velocity distribution, with less dramatic fluctuations and a maximum velocity of around 0.038 m/s. Such a steady airflow is essential for uniform drying because it ensures that the drying medium, likely hot air, moves more predictably and consistently through the drying chamber. This consistency minimizes the risk of localized over-drying or under-drying, providing a more even drying process across the material being dried. In contrast, graph in Figure 4.13, with its higher and more variable velocity, suggests more turbulent and uneven airflow, which could lead to inconsistent drying results.

4.2.1.6 Velocity variation analysis for third design of the solar dryer

Graphs in Figures (4.17 and 4.18) compare the velocity distribution inside the third design of a direct solar dryer at two different points (left and right lower ends respectively) over time. Graph in Figure 4.17 shows a significant increase in velocity, peaking around 0.36 m/s at approximately 60 seconds, followed by slight fluctuations. This indicates a strong airflow at this point, suggesting efficient drying conditions. Graph in Figure 4.18, however, shows lower overall velocities, peaking at 0.055 m/s around 40 seconds, with noticeable oscillations throughout the time period. This suggests that the

airflow at the second point is less stable and weaker compared to the first point, indicating potential areas for improvement in the drying efficiency at this location.

Graph in Figure 4.17 indicates better uniform drying due to its relatively stable and consistent increase in velocity over time, peaking at a higher velocity (around 0.36 m/s) with fewer fluctuations compared to graph in Figure 4.18. The higher and more stable airflow suggests that the drying process is more efficient and uniform at the left lower end of the dryer, as a consistent airflow can more effectively remove moisture from the material being dried. In contrast, graph in Figure 4.18 shows more variability and lower peak velocities, indicating less efficient and more uneven drying conditions at the right lower end of the dryer.

Chapter 5

Conclusions and Recommendations

5.1 Conclusions

The study utilized Computational Fluid Dynamics (CFD) to evaluate and compare the performance of three different designs of agricultural direct solar dryers. The analysis focused on airflow patterns, temperature distributions, and drying efficiency to determine the optimal design for agricultural applications. Key conclusions derived from the study include:

Airflow Patterns: The simulations revealed significant differences in airflow patterns among the three dryer designs. The first design exhibited non-uniform airflow with several dead zones, which could lead to uneven drying. The second and third designs showed improved airflow uniformity, with the third design demonstrating the most consistent
airflow distribution.

Temperature Distribution: Temperature distribution analysis indicated that the third design achieved a more uniform and stable temperature profile across the drying chamber. This design minimized temperature fluctuations and provided a steady heat distribution, which is crucial for efficient and consistent drying of agricultural products.

Drying Efficiency: The comparative analysis of drying efficiency highlighted that the third design outperformed the others. The steady and uniform airflow, combined with consistent temperature distribution, contributed to better moisture removal and reduced drying times.

Design Optimization: The study underscored the importance of geometric design and the positioning of air inlets and outlets in achieving optimal dryer performance. Design adjustments that promote uniform airflow and stable temperature distribution can significantly enhance the efficiency of solar dryers.

In conclusion, the third design of the agricultural direct solar dryer, characterized by its optimized airflow and temperature distribution, is recommended as the most efficient and effective solution for agricultural drying applications. This design promises improved drying performance, reduced post-harvest losses, and better preservation of agricultural products.

5.2 Recommendations and Future Work

Based on the findings and conclusions of this study, several recommendations and areas for future research are proposed:

1. It is recommended to implement the third dryer design in real-world settings and conduct experimental testing to validate the CFD simulation results. Practical trials will provide valuable data on the actual performance, reliability, and scalability of the design.

2. Future research should explore the use of different materials for constructing the solar dryers. Materials that enhance thermal efficiency, durability, and cost-effectiveness should be identified and tested to optimize the overall performance and economic feasibility of the dryers.

3. Investigate additional methods to improve the energy efficiency of the solar dryers. Incorporatingadvancedsolarenergycollectiontechniques,

suchassolarconcentrators or photovoltaic panels, could enhance the energy capture and utilization, further reducing drying times and operational costs.

4. Developing and integrating automation and control systems into the solar dryers Chapter 5. Conclusions and Recommendations

   could enhance their performance. Automated systems that monitor and adjust airflow, temperature, and humidity levels can ensure optimal drying conditions and improve the quality of the dried products.

5. Conduct a comprehensive economic analysis to evaluate the cost-benefit ratio of the optimized dryer design. This analysis should consider the initial investment, operational costs, maintenance, and potential revenue from the improved drying process to provide a clear picture of the economic viability for farmers and stakeholders.

6. Assess the environmental impact of the solar dryers, focusing on their contribution to reducing carbon emissions and reliance on non-renewable energy sources. Highlighting the environmental benefits can support the adoption of sustainable drying technologies in the agricultural sector.

By addressing these recommendations and pursuing further research, the development and optimization of agricultural direct solar dryers can be advanced, leading to more efficient, sustainable, and economically viable solutions for post-harvest processing.

References

Adeniyi, A. A., Mohammed, A., & Aladeniyi, K. (2012). Analysis of a solar dryer box with ray tracing cfd technique. *International Journal of Scientific & Engineering Research*, *3*(10), 1–5.

Adnouni, M., Jiang, L., Zhang, X., Zhang, L., Pathare, P. B., & Roskilly, A. (2023). Computational modelling for decarbonised drying of agricultural products:

Sustainable processes, energy efficiency, and quality improvement. *Journal of Food Engineering*, *338*, 111247.

Amit, S. K., Uddin, M. M., Rahman, R., Islam, S. R., & Khan, M. S. (2017). A review on mechanisms and commercial aspects of food preservation and processing. *Agriculture & Food Security*, *6*, 1–22.

Babu, A. K., Kumaresan, G., Raj, V. A. A., & Velraj, R. (2018). Review of leaf drying: Mechanism and influencing parameters, drying methods, nutrient preservation, and mathematical models. *Renewable and sustainable energy reviews*, *90*, 536–556.

Behera, D. D., Mohanty, R. C., & Mohanty, A. M. (2023). Thermal performance of a hybrid solar dryer through experimental and cfd investigation. *Journal of Food Process Engineering*, *46*(8), e14386.

Benhamza, A., Boubekri, A., Atia, A., Hadibi, T., & Arıcı, M. (2021). Drying uniformity analysis of an indirect solar dryer based on computational fluid dynamics and image processing. *Sustainable Energy Technologies and Assessments*, *47*, 101466.

Chaudhari, V. D., Kulkarni, G. N., & Sewatkar, C. M. (2021). Computational fluid dynamics analysis of cabinet-type solar dryer. *Journal of Food Process Engineering*, *44*(8), e13756.

Chauhan, P. S., Kumar, A., & Tekasakul, P. (2015). Applications of software in solar drying systems: A review. *Renewable and Sustainable Energy Reviews*, *51*, 1326–1337.

Chavan, A., Vitankar, V., Shinde, N., & Thorat, B. (2021). Cfd simulation of solar grain dryer. *Drying Technology*, *39*(8), 1101–1113.

Crist, E., Mora, C., & Engelman, R. (2017). The interaction of human population, food

production, and biodiversity protection. *Science*, *356*(6335), 260–264.

Defraeye, T. (2014). Advanced computational modelling for drying processes–a review. *Applied Energy*, *131*, 323–344.

Demissie, P., Hayelom, M., Kassaye, A., Hailesilassie, A., Gebrehiwot, M., & Vanierschot, M. (2019). Design, development and cfd modeling of indirect solar food dryer. *Energy Procedia*, *158*, 1128–1134.

El-Mesery, H. S., El-Seesy, A. I., Hu, Z., & Li, Y. (2022). Recent developments in solar drying technology of food and agricultural products: A review. *Renewable and Sustainable Energy Reviews*, *157*, 112070.

Getahun, E., Delele, M. A., Gabbiye, N., Fanta, S. W., Demissie, P., & Vanierschot, M. (2021). Importance of integrated cfd and product quality modeling of solar dryers for fruits and vegetables: A review. *Solar Energy*, *220*, 88–110.

Ghaffari, A., & Mehdipour, R. (2015). Modeling and improving the performance of cabinet solar dryer using computational fluid dynamics. *International journal of food engineering*, *11*(2), 157–172.

Goel, V., Dwivedi, A., Mehra, K. S., Pathak, S. K., Tyagi, V., Bhattacharyya, S., & Pandey, A. (2024). Solar drying systems for domestic/industrial purposes: A state-of-art review on topical progress and feasibility assessments. *Solar Energy*, *267*, 112210.

Güler, H. Ö., Sözen, A., Tuncer, A. D., Afshari, F., Khanlari, A., Şirin, C., & Gungor, A. (2020). Experimental and cfd survey of indirect solar dryer modified with low-cost iron mesh. *Solar Energy*, *197*, 371–384.

Holechek, J. L., Geli, H. M., Sawalhah, M. N., & Valdez, R. (2022). A global assessment: can renewable energy replace fossil fuels by 2050? *Sustainability*, *14*(8), 4792.

Iranmanesh, M., Akhijahani, H. S., & Jahromi, M. S. B. (2020). Cfd modeling and evaluation the performance of a solar cabinet dryer equipped with evacuated tube solar collector and thermal storage system. *Renewable Energy*, *145*, 1192–1213.

References

Jain, A., Sharma, M., Kumar, A., Sharma, A., & Palamanit, A. (2019). Computational fluid dynamics simulation and energy analysis of domestic direct-type multi-shelf solar dryer. *Journal of Thermal Analysis and Calorimetry*, *136*, 173–184.

Malekjani, N., & Jafari, S. M. (2018). Simulation of food drying processes by computational fluid dynamics (cfd); recent advances and approaches. *Trends in food science & technology*, *78*, 206–223.

Marten, G. G. (2010). *Human ecology: Basic concepts for sustainable development*. Routledge.

Mohana, Y., Mohanapriya, R., Anukiruthika, T., Yoha, K., Moses, J., & Anandharamakrishnan, C. (2020). Solar dryers for food applications: Concepts, designs, and recent advances. *Solar Energy*, *208*, 321–344.

Mukanema, M., & Simate, I. N. (2023). Cfd simulation of temperature and air flow in a natural convection solar tunnel dryer with a bare flat-plate chimney. *Energy and Environment Research*, *13*(1).

Ndukwu, M. C., Ibeh, M., Ekop, I., Abada, U., Etim, P., Bennamoun, L., . . . Gupta, A. (2022). Analysis of the heat transfer coefficient, thermal effusivity and mathematical modelling of drying kinetics of a partitioned single pass low-cost solar drying of cocoyam chips with economic assessments. *Energies*, *15*(12), 4457.

Noh, A. M., Mat, S., & Ruslan, M. H. (2018). Cfd simulation of temperature and air flow distribution inside industrial scale solar dryer. *Journal of Advanced Research in Fluid Mechanics and Thermal Sciences*, *45*(1), 156–164.

Obayopo, S. O., & Oluwasanmi, A. (2019). Cfd and experimental analysis of direct solar dryer for fish. *Agricultural Engineering International: CIGR Journal*, *21*(2), 108–117.

Ortiz-Rodríguez, N., Condorí, M., Durán, G., & García-Valladares, O. (2022). Solar drying technologies: A review and future research directions with a focus on agroindustrial applications in medium and large scale. *Applied Thermal Engineering*, *215*, 118993.

References

Pandey, S., Kumar, A., & Sharma, A. (2024). Sustainable solar drying: Recent advances in materials, innovative designs, mathematical modeling, and energy storage solutions. *Energy*, 132725.

Pawlak, K., & Kołodziejczak, M. (2020). The role of agriculture in ensuring food security in developing countries: Considerations in the context of the problem of sustainable

food production. *Sustainability*, *12*(13), 5488.

Prakash, O., Laguri, V., Pandey, A., Kumar, A., & Kumar, A. (2016). Review on various modelling techniques for the solar dryers. *Renewable and Sustainable Energy Reviews*, *62*, 396–417.

Runganga, T. B. (2019). *A solar crop dryer for rural areas* (Unpublished doctoral dissertation). Cape Peninsula University of Technology.

Sadeghi, G., Taheri, O., & Mobadersani, F. (2012). New technologies of solar drying systemsforagriculturalandmarineproducts. In*The1stmiddle-eastdryingconference (medc2012), mahshar, iran.*

Sahdev, R. K. (2014). Open sun and greenhouse drying of agricultural and food products: a review. *International Journal of Engineering Research*, *3*(3).

Sanghi, A., Ambrose, R. K., & Maier, D. (2018). Cfd simulation of corn drying in a natural convection solar dryer. *Drying technology*, *36*(7), 859–870.

Schobeiri, M. T. (2010). *Fluid mechanics for engineers: a graduate textbook*. Springer Science & Business Media.

Sharma, A., Chen, C., & Lan, N. V. (2009). Solar-energy drying systems: A review. *Renewable and sustainable energy reviews*, *13*(6-7), 1185–1210.

Singh, R., Salhan, P., & Kumar, A. (2021). Cfd modelling and simulation of an indirect forced convection solar dryer. In *Iop conference series: Earth and environmental science* (Vol. 795, p. 012008).

References

Sonthikun, S., Chairat, P., Fardsin, K., Kirirat, P., Kumar, A., & Tekasakul, P. (2016). Computational fluid dynamic analysis of innovative design of solar-biomass hybrid dryer: An experimental validation. *Renewable Energy*, *92*, 185–191.

Ssemwanga, M., Makule, E., & Kayondo, S. (2020). Performance analysis of an improved solar dryer integrated with multiple metallic solar concentrators for drying fruits. *Solar Energy*, *204*, 419–428.

Stoppe, A. C. R., Neto, J. L. V., & dos Santos, K. G. (2020). Development of a fixed bed solar dryer: experimental study and cfd simulation. *Research, Society and Development*, *9*(3), e123932667–e123932667.

Tadesse, M. (2020). Post-harvest loss of stored grain, its causes and reduction strategies. *Food Science and Quality Management*, *96*, 26–35.

Tiwari, A. (2016). A review on solar drying of agricultural produce. *Journal of Food Processing & Technology*, *7*(9), 1–12.

Tu, J., Yeoh, G. H., Liu, C., & Tao, Y. (2023). *Computational fluid dynamics: a practical approach*. Elsevier.

Visavale, G. (2012). Principles, classification and selection of solar dryers. *Solar drying: Fundamentals, Applications and Innovations, Ed. Hii, CL, Ong, SP, Jangam, SV and Mujumdar, AS, Published in Singapore*, 1–50.

Vivekanandan, M., Periasamy, K., Babu, C. D., Selvakumar, G., & Arivazhagan, R. (2021). Experimental and cfd investigation of six shapes of solar greenhouse dryer in no load conditions to identify the ideal shape of dryer. *Materials Today: Proceedings*, *37*, 1409–1416.

Yunus, Y., & Al-Kayiem, H. H. (2013). Simulation of hybrid solar dryer. In *Iop conference series: Earth and environmental science* (Vol. 16, p. 012143).